# Fundamental aspects of arm repair phase in two echinoderm models

Cinzia Ferrario[a,b,1], Yousra Ben Khadra[c], Anna Czarkwiani[d], Anne Zakrzewski[d], Pedro Martinez[e,f], Graziano Colombo[a], Francesco Bonasoro[a,1], Maria Daniela Candia Carnevali[a,1], Paola Oliveri[d], Michela Sugni[a,b,1*]

[a] Dipartimento di Bioscienze, Università degli Studi di Milano, via Celoria, 26, 20133, Milano, Italy

[b] Center for Complexity & Biosystems, Dipartimento di Fisica, Università degli Studi di Milano, via Celoria, 16, 20133, Milano, Italy

[c] Laboratoire de Recherche, Génétique, Biodiversité et Valorisation des Bioressources, Institut Supérieur de Biotechnologie de Monastir, Université de Monastir, Monastir, Tunisia

[d] Department of Genetics, Evolution and Environment, University College London, Darwin Building, Gower Street, WC1E 6BT, London, United Kingdom

[e] Departament de Genètica, Microbiologia I Estadística, Universitat de Barcelona, Av. Diagonal, 645, E-08028 Barcelona, Spain

[f] ICREA (Institut Català de Recerca i Estudis Avancats), Barcelona, Spain

[1] Dipartimento di Scienze e Politiche Ambientali, Università degli Studi di Milano, via Celoria, 2, 20133, Milano, Italy

* Corresponding author: michela.sugni@unimi.it; Dipartimento di Scienze e Politiche Ambientali, Università degli Studi di Milano, via Celoria, 2, 20133, Milano, Italy.

*Authors' e-mail contacts:*

CF: cinzia89.ferrario@alice.it

YBK: youssra_benkhadra@yahoo.fr

AC: a.czarkwiani@ucl.ac.uk

AZ: a.zakrzewski@ucl.ac.uk

PM: pedro.martinez@ub.edu

GC: graziano.colombo@unimi.it

FB: francesco.bonasoro@unimi.it

MDCC: daniela.candia@unimi.it

PO: p.oliveri@ucl.ac.uk

MS: michela.sugni@unimi.it

***Abstract***

Regeneration is a post-embryonic developmental process that ensures complete morphological and functional restoration of lost body parts. The repair phase is a key step for the effectiveness of the subsequent regenerative process: in vertebrates, efficient re-epithelialisation, rapid inflammatory/immune response and post-injury tissue remodelling are fundamental aspects for the success of this phase, their impairment leading to an inhibition or total prevention of regeneration. Among deuterostomes, echinoderms display a unique combination of striking regenerative abilities and diversity of useful experimental models, although still largely unexplored.

Therefore, the brittle star *Amphiura filiformis* and the starfish *Echinaster sepositus* were here used to comparatively investigate the main repair phase events after injury as well as the presence and expression of immune system and extracellular matrix (*i.e.* collagen) molecules using both microscopy and molecular tools.

Our results showed that emergency reaction and re-epithelialisation are similar in both echinoderm models, being faster and more effective than in mammals. Moreover, in comparison to the latter, both echinoderms showed delayed and less abundant collagen deposition at the wound site (absence of fibrosis). The gene expression patterns of molecules related to the immune response, such as *Ese-fib-like* (starfishes) and *Afi-ficolin* (brittle stars), were described for the first time during echinoderm regeneration providing promising starting points to investigate the immune system's role in these regeneration models.

Overall, the similarities in repair events and timing within the echinoderms and the differences with what has been reported in mammals suggests that effective repair processes in echinoderms play an important role for the subsequent ability to regenerate. Targeted molecular and functional analyses will shed light on the evolution of these abilities in the deuterostomian lineage.

**Keywords:** starfishes; brittle stars; emergency reaction; wound healing; collagen; immune/inflammatory response.

**Highlights**

- Echinoderms are valid models to study repair phase and regeneration post amputation

- Quick re-epithelialisation and wound contraction characterise echinoderm wound healing
- Echinoderm epidermis has a multi-functional role during the repair phase
- Delayed collagen deposition and no fibrosis differentiate echinoderms from mammals

## *1. Introduction*

All animals face and heal wounds regardless of their phylogenetic position and the life stage of individuals, though the final result of the restoration process can be remarkably different. The first post-traumatic events and the specific regulation and cross talk of the numerous cytotypes and molecules involved are fundamental to address the final outcome: tissue repair *versus* tissue regeneration and functional recovery (White *et al.*, 2009). In vertebrates, the main steps of wound repair are re-epithelialisation, inflammatory/immune response, formation of the granulation tissue, and extracellular matrix (ECM) deposition and remodelling (Xue and Jackson, 2015). The impairment of these events, such as the absence/reduction of re-epithelialisation, the misregulation of the inflammatory/immune response and the occurrence of fibrosis, can be correlated with limited regenerative ability.

Wound healing *via* a complete and functional epithelial layer is a critical step to ensure effective repair (Pastar *et al.*, 2014): for example, in mammals impaired epidermal restoration leads to chronic non-healing wounds, causing severe medical problems such as ulcers and absence of tissue regeneration (Sivamani *et al.*, 2007).

Functional repair is achieved also thanks to a highly tuned inflammatory and immune response. The immune system is fundamental during haemostasis and throughout the whole inflammation phase (Park and Barbul, 2004; MacLeod and Mansbridge, 2015). In mammals, several molecules, such as fibrinogen, lectins, ficolins, cytokines (*i.e.* TNF-α and TGF-β) and interleukins (*i.e.* IL-1, Il-2, IL-6, IL-8), are key players during the inflammation process and their misregulation as well as local and systemic factors, may affect proper wound healing (Guo and DiPietro, 2006) and subsequent tissue restoration.

The constant and finely regulated remodelling of the ECM components (mainly collagen) is a further key event needed for effective wound healing (Xue and Jackson, 2015). Exaggerated inflammatory response during the first phase of repair can lead to fibro-proliferative disorders (Tredget *et al.*, 1997; Singer and Clark, 1999) which in turn result in excessive deposition of collagen and other ECM molecules (fibrosis) (Ben Amar and Bianca, 2016) and occasionally also in pathological hypertrophic scar or keloid formation. Over-deposition of collagen and its reduced remodelling are known to impair proper healing and

regeneration of the damaged tissues (Bock and Mrowietz, 2002; Rahban and Garner, 2003; Diegelmann and Evans, 2004).

It is noteworthy that vertebrates are able to heal minor injuries but most of them possess restricted ability to completely restore lost body parts (Sánchez Alvarado, 2000). Some fishes (Akimenko *et al.*, 2003), amphibian urodeles (Brockes and Kumar, 2002) and reptiles (Bateman and Fleming, 2009) can repair and regenerate after severe or debilitating wounds but the most striking regenerative abilities are still and by far found among the invertebrate clades. Cnidarians (Bosch, 2007), planarians (Saló *et al.*, 2009), annelids (Bely, 2006), and echinoderms (Candia Carnevali, 2006) are the most representative examples. Echinoderms (Arnone *et al.*, 2015) in particular show the maximum extent of regenerative potential among deuterostomes: indeed, they can regenerate body appendages such as arms (Candia Carnevali, 2006), internal organs (Mozzi *et al.*, 2006; Mashanov and García-Arrarás, 2011), and even whole animals from an isolated body fragment (Ducati *et al.*, 2004). Moreover, representatives of all the five extant classes display regenerative capabilities (Hyman, 1955) with clear examples also found in fossils (Oji, 2001), suggesting that these are ancient and widespread features of the phylum. Therefore, echinoderms are promising models to study this phenomenon and, thus, they provide us with a valid comparative perspective with non-regenerating models, humans included.

Arm regeneration is one of the most extensively studied processes in echinoderms (for a review see Candia Carnevali and Bonasoro, 2001; Biressi *et al.*, 2010; Ben Khadra *et al.*, 2017). Regardless of the species, different critical events take place during the first hours/days post amputation, including wound closure, re-epithelialisation and a rapid inflammatory response. As for mammals (Stroncek and Reichert, 2008), tissue remodelling at the wound site is also observed. During sea cucumber gut regeneration tissue remodelling is one of the last phenomena occurring in the repair phase and this was suggested to be directly related to their high efficiency of regeneration (Quiñones *et al.*, 2002; Cabrera-Serrano and García-Arrarás, 2004). Furthermore, immune-related molecules have been described in sea urchins and sea cucumbers (Pancer *et al.*, 1999; Rast *et al.*, 2006; Ramírez-Gómez *et al.*, 2008, 2009, 2010; Ramírez-Gómez and García-Arrarás, 2010; Smith *et al.*, 2010) and their presence/role needs to be comparatively investigated in the repair processes of other echinoderms. This should lead to a deeper understanding of the process and to shed light on evolutionary divergences/similarities within the phylum and with non-regenerating models.

Among the different echinoderm models, starfishes (Asteroidea) and brittle stars (Ophiuroidea) are becoming valid experimental models to study arm regenerative process (Ben Khadra *et al.*, 2017; Biressi *et al.*, 2010; Czarkwiani *et al.*, 2013, 2016). Nevertheless, in both classes, the cellular/tissue and molecular aspects of the repair phase have never been simultaneously and comparatively investigated and with a multidisciplinary approach. Therefore, this research aims to describe and compare the phenomena occurring during the repair phase after traumatic arm amputation using both the brittle star *Amphiura filiformis* (Ophiuroidea) and the starfish *Echinaster sepositus* (Asteroidea). Classical histological and ultrastructural methods are employed for the description of the main repair events from a cell/tissue perspective, whereas molecular techniques are used to investigate the involvement of inflammatory/immune responses and the ECM (mainly collagen). Overall, a detailed knowledge on how echinoderms heal severe wounds, and actually regenerate, will possibly shed light on similarities and/or differences with other animals able to regenerate whole lost body parts and, also, with those unable to do it, humans included.

## *2. Materials and Methods*

### *2.1. Animal collection, maintenance and regeneration tests*

Adult (disc diameter ~ 0.5 cm) specimens of *Amphiura filiformis* were collected at the Sven Lovén Centre for Marine Sciences in Kristineberg (Sweden). Adult (diameter ~ 12 cm) specimens of *Echinaster sepositus* were collected by SCUBA divers at depth of 5-8 m in the Marine Protected Areas of Portofino (Ligurian Sea, Italy) and of Bergeggi Island (Ligurian Sea, Italy). All experimental animals were left to acclimatise for about one-two weeks and maintained in aerated aquaria of artificial sea water (ASW) (Instant Ocean®) at 14°C and 34‰ salinity (brittle stars) or 18°C and 37‰ salinity (starfishes). Chemical-physical ASW parameters were constantly checked. Animals were fed twice a week with Microvore Microdiet (Brightwell Aquatics; brittle stars) or small pieces of cuttlefish (starfishes). Traumatic arm amputation was performed using a scalpel: for brittle stars a maximum of two arms per animal were amputated at 1 cm from the disc, whereas for starfishes the distal third of one arm was removed. Brittle stars were previously anaesthetised in 3.5% $MgCl_2$ ($6H_2O$) solution (pH 8.3) in a 1:1 mix of filtered ASW and milliQ water. Animals were then left to regenerate in the aquaria for pre-determined periods, namely 24 and 72 hours (h) and 1 week (w) post-amputation (p.a.) for *E. sepositus* and 8, 16, 24, 48, 72 hours (h) and 5 days (d) p.a. (corresponding to stage 2 of Czarkwiani *et al.*, 2016) for *A. filiformis*. Brittle star samples at 8d (stage 4) and 2-3 weeks (w) p.a. (>50% DI; Dupont and Thorndyke, 2006;

170 from now on called >50%) were collected and processed as well in order to confirm/complete
171 some *in situ* hybridisation results (see below and Supplementary Materials). Regenerating
172 arms were collected including part of the stump and differently processed according to the
173 subsequent analyses.
174
175 ***2.2. Microscopy analyses***
176 *2.2.1. Light (LM) and transmission electron microscopy (TEM)*
177 For Epon resin embedding regenerating samples were fixed in 2% glutaraldehyde in 0.1 M
178 sodium cacodylate (pH about 7.4) with 1.2% (brittle stars) or 1.4% (starfishes) NaCl and
179 washed overnight at 4°C in 0.1 M cacodylate buffer. They were then processed as described
180 by Ben Khadra and co-workers (2015a) with only slight modifications in decalcification step
181 that was performed after osmium tetroxide post-fixation at 4°C for at least 2-3 days using a
182 1:1 solution (v/v) of 2% L-ascorbic acid and 0.3 M NaCl in distilled water. Semi-thin sections
183 (1 µm) were obtained using a Reichert-Jung Ultracut E with glass knives, stained with crystal
184 violet and basic fuchsin and then observed under a Jenaval light microscope provided with
185 a DeltaPix Invenio 3S 3M CMOS camera and DeltaPix Viewer LE Software or a Zeiss
186 AxioImager M1 microscope equipped with a Zeiss AxioCamHRc camera.
187 For transmission electron microscopy (TEM) the same samples used for semi-thin sections
188 were used to obtain ultra-thin sections (0.07-0.1 µm) which were collected on copper grids,
189 stained with 1% uranyl acetate followed by lead citrate and finally carbon coated with an
190 EMITECH K400X Carbon Coater. Grids were observed and photographed using a Jeol
191 100SX, a Zeiss EFTEM Leo912ab or a PHILIPS CM 10 transmission electron microscope.
192
193 ***2.3. Gene expression analyses***
194 Gene expression analysis is of paramount importance to understand the process of wound
195 healing and regeneration; however, little or no protocols have been so far adapted to detect
196 genes expressed during starfish regeneration. To optimise and validate the protocols of ISH
197 on paraffin sections for starfishes, two genes were identified and cloned (see below): an
198 *actin* gene (*Ese-actin*) and the transcription factor *ets1/2* (*Ese-ets1/2*). The same genes
199 were selected as positive controls also for WMISH on brittle star samples: *Afi-actin* was
200 identified and cloned for the first time, whereas *Afi-ets1/2* was already available (Czarkwiani
201 *et al.*, 2013). For all the positive controls specific fragments were isolated by PCR and cloned
202 in bacteria vector to transcribe antisense RNA probes, as detailed below and in the
203 Supplementary Materials.

204

205 *2.3.1. Candidate gene identification*

206 Gene identification in both species was performed looking for markers of the regenerative
207 process with a specific focus on those involved in the collagen deposition regulation and the
208 immune/inflammatory response during the repair phase. Since it was not always possible to
209 clone the candidate genes in both species, we will show the data of different markers (see
210 below).

211

212 *2.3.1.1. Candidate gene identification in E. sepositus*

213 The identified gene of interest was the collagen biosynthesis enzyme *prolyl-4-hydroxylase*
214 (*p4h*). Due to the absence of any transcriptome for this species, degenerate primers (see
215 Table S2) were manually designed on protein multialignment built on sequences retrieved
216 from EchinoBase for *Strongylocentrotus purpuratus* and *Patiria miniata* genomes, and
217 EchinoDB (http://echinodb.uncc.edu/) and National Center for Biotechnology Information
218 (NCBI) databases. After cloning a specific fragment by PCR using these primers, *Ese-p4h*
219 sequence was checked performing a Basic Local Alignment Search Tool (BLAST) against
220 the NCBI non-redundant database (https://blast.ncbi.nlm.nih.gov/Blast.cgi), identifying as
221 best BLAST hit the alpha-1 subunit of the Atlantic herring (*Clupea harengus*,
222 XP_012689665.1; Table S1). Furthermore, the conserved domain architecture retrieval tool
223 (cDART, NCBI) showed the 2OG-Fe(II) oxygenase superfamily domain is encoded on the
224 *Ese-p4h* isolated fragment. This domain is characteristic of P4H therefore confirming it was
225 the desired collagen biosynthesis enzyme.

226 Degenerate primers from Zhang and Cohn (2006) for vertebrate collagen were tested as
227 well (see Table S2). *Ese-fibrinogen-like* (*Ese-fib-like*) is a gene belonging to the fibrinogen-
228 related (FReD) domain superfamily. Using the cDART tool (NCBI) the presence of a FReD
229 domain was confirmed. This is usually present in fibrinogen, a glycoprotein that helps in the
230 formation of blood clotting in vertebrates forming bridges between platelets and being the
231 precursor of fibrin.

232 As previously mentioned, *actin 1* and *ets1/2* were selected as positive controls: specific
233 primers were designed based on the nucleotide sequence of *actin 1* (NCBI accession
234 number: KC858258.1, GI: 525327359; see Supplementary Materials), whereas degenerate
235 primers already available in the laboratory were used to clone *ets1/2* (see Table S2). For
236 *actin 1*, since the expected product length was shorter than 300 bp, 3'RACE was performed
237 using a mixed cDNA samples from regenerate stages with the FirstChoice® RLM-RACE Kit

238 (Ambion) according to manufacturer's instructions (see Supplementary Materials and Table
239 S3). We cloned a longer fragment that was used to obtain a longer RNA antisense probe for
240 *in situ* hybridisation (see below). Table S1 summarises the best BLAST hits of the identified
241 genes in EchinoBase (SPU best BLAST) and in NCBI (NCBI best BLAST).
242
243 *2.3.1.2. Candidate gene identification in A. filiformis*
244 Genes of interest were identified from EchinoBase (http://www.echinobase.org), starting
245 with a targeted gene search in *Strongylocentrotus purpuratus* database
246 (http://www.echinobase.org/Echinobase/) using Gene Name or Gene Synonym as
247 searching words. BLAST-X analyses were performed over the *Afi* transcriptome (Dylus *et*
248 *al.*, 2017) in order to obtain the corresponding gene sequences in *A. filiformis*. The genes of
249 interest were *Afi-p4h* and *Afi-ficolin*, whereas *actin* (*Afi-actin*) was used as positive control
250 (see Supplementary Materials).
251 The *Afi-p4h* (AfiCDS.id43946.tr460) similarly identified as best BLAST hit in the sea urchin
252 genome (EchinoBase; http://www.echinobase.org/Echinobase/) the prolyl-4-hydroxylase
253 alpha-1 subunit precursor (SPU_027669), whereas in the NCBI non-redundant database
254 the Atlantic herring prolyl-4-hydroxylase subunit alpha-1 (*Clupea harengus*,
255 XP_012689665.1). The cDART tool confirmed the presence of a prolyl-4-hydroxylase alpha
256 subunit domain. Therefore, this transcript was considered as prolyl-4-hydroxylase (*p4h*).
257 The *Afi-ficolin* gene (*Afi*CDS.id39565.tr647) was isolated from an *A. filiformis* cDNA pool.
258 The clone sequence was analysed using BLAST-X against the sea urchin genome (*S.*
259 *purpuratus*; EchinoBase) and NCBI non-redundant database and confirmed to belong to the
260 FReD superfamily and to be a closely related gene to the sea urchin *Sp-Fic1* (SPU_000045).
261 Table S1 summarises the best BLAST hits of the identified genes in EchinoBase (SPU best
262 BLAST) and in NCBI (NCBI best BLAST) with corresponding scores and E-values.
263
264 *2.3.2. Primer design*
265 Different design strategies were followed depending on the gene of interest and sequence
266 availability. For specific primers in both species PRIMER3 Software version 0.4.0
267 (http://primer3.ut.ee/) was used, optimising the following parameters: max 3' stability was
268 set at 8.0 and max polyX at 3. For brittle stars their specificity was checked performing a
269 BLAST to the *A. filiformis* developmental transcriptome (Dylus *et al.*, 2017). Degenerate
270 primers were manually designed as described above. Tables S2 and S3 summarises all *E.*
271 *sepositus* and *A. filiformis* primers.

272

273 *2.3.3. RNA extraction, cDNA synthesis, gene cloning and antisense probe transcription*

274 For *A. filiformis,* RNA was extracted, genes were cloned and antisense probes were
275 prepared as described by Czarkwiani and co-workers (2013). RNA of *E. sepositus* was
276 extracted at the different regenerating stages (24 hours, 72 hours and one week p.a.) from
277 5 specimens per stage with the RiboPure Kit (Ambion) following manufacturer's instructions.
278 cDNA synthesis was performed using the RETROscript kit (Ambion) following
279 manufacturer's instructions and using 1 µg of total RNA. A pool of cDNA was prepared and
280 used to perform subsequent PCRs. The amplification reaction protocol using Invitrogen
281 reagents (*Taq* DNA Polymerase (Invitrogen) or Q5 High-Fidelity DNA Polymerase (New
282 England BioLabs)) was optimised for each gene of interest (see Supplementary Materials).
283 Moreover, when necessary 3'RACE was performed (see Supplementary Materials). All PCR
284 products were subsequently ligated into pGEM®-T Easy Vector System I (Promega) and
285 transformed in Subcloning Efficiency Invitrogen DH5α (Life Technologies) or Top 10
286 Competent Cells *E. coli* (Fisher Scientific) according to manufacturer's instructions. The
287 presence of the correct fragment was checked by sequencing (Source BioScience). RNA
288 antisense digoxigenin (DIG) labelled probes were transcribed *in vitro* using the Sp6/T7
289 Transcription Kit (Roche) and the DIG RNA labelling Mix (Roche) following manufacturer's
290 guidelines.

291

292 *2.3.4. Whole mount in situ hybridisation (WMISH) on A. filiformis*

293 Brittle star *in situ* hybridisations were performed in whole mount and then samples were
294 embedded in paraffin wax and sectioned for detailed analysis. *A. filiformis* regenerating
295 samples were fixed in 4% PFA in 1X PBS with 0.1% Tween-20 (PBST) overnight at 4°C and
296 stored in 100% methanol at -20°C until use.

297 Chromogenic WMISH was performed with antisense probes as previously described along
298 with positive and negative controls (Czarkwiani *et al.*, 2013) with the following modifications:
299 hybridisation temperature was raised to 50-55°C depending on the probe length and all
300 washes were conducted in 1X MABT (0.1 M maleic acid pH 7.5, 0.15 M NaCl, 0.1% Tween-
301 20). Samples were stored in 50% glycerol at 4°C and subsequently observed under a Zeiss
302 AxioImager M1 microscope equipped with a Zeiss AxioCam HRc camera.

303 After imaging, WMISH samples were embedded in paraffin wax and sectioned in order to
304 better understand the tissue-specific expression patterns. Briefly, samples stored in 50%
305 glycerol were washed in 1x PBS or 1x MABT at room temperature (RT) and decalcified for

306 1-2 days in 0.5 M EDTA in 1x PBS (pH 8) or in 1:1 solution (v/v) of 2% L-ascorbic acid and
307 0.3 M NaCl in distilled water at 4°C. After washes in 1x PBS or 1x MABT, they were post-
308 fixed in 4% PFA in 1x PBS or 2% glutaraldehyde in 1x MABT at RT, washed twice in 1x PBS
309 or 1x MABT, de-hydrated in an increasing scale of ethanol, cleared in xylene and embedded
310 in paraffin wax following classical procedures. Samples were then sectioned (10 µm
311 thickness) and sections were de-waxed in xylene, mounted with Eukitt® and observed under
312 a Jenaval light microscope provided with a DeltaPix Invenio 3S 3M Pixel CMOS camera and
313 DeltaPix ViewerLE Software.
314
315 *2.3.5. In situ hybridisation (ISH) on E. sepositus sections*
316 Because of the limited number of starfish regenerating arm samples, their large size (around
317 1 cm) and the bright orange pigmentation typical of this species, an ISH on paraffin wax
318 sections was optimised. Samples were fixed in 4% PFA in 0.1 M MOPS (pH 7) and 0.5 M
319 NaCl for at least one week at 4°C or in 4% PFA in PBST, decalcified in Morse's solution
320 (10% sodium citrate and 20% formic acid in DEPC-treated water) overnight at 4°C and
321 embedded in paraffin wax as described by Ben Khadra and co-workers (2015a). Samples
322 were sectioned at 10 µm thickness using a Leica RM2155 microtome. Since no ISH
323 technique is reported in the literature for *E. sepositus* paraffin sections, two different
324 protocols were tested and optimised, giving us comparable results. In parallel, negative
325 controls were run performing the hybridisation without probes in order to check potential
326 anti-DIG antibody cross-reactivity. ISH protocols are detailed in the Supplementary
327 Materials. After ISH, sections were imaged under a Zeiss AxioImager M1 microscope
328 equipped with a Zeiss AxioCamHRc camera.
329
330 ***3. Results***
331 A brief description of the gross morphology of starfish and brittle star arms is re-called in the
332 Supplementary Materials to facilitate the understanding of the subsequent results (Fig. S1).
333 Since the epidermis plays a key role during the repair phase (see below) and no data is
334 currently available for *Amphiura filiformis*, a new ultrastructural description of the non-
335 regenerating epidermis is here briefly provided. For the description of the non-regenerating
336 epidermis of *Echinaster sepositus* see Ben Khadra and co-workers (2015a).
337 In *A. filiformis*, the aboral and oral epidermis lines the trabeculae of the skeletal shields (Fig.
338 1A, B, C). This epithelium is composed of an external cuticle, the epidermal cells and the
339 underlying basal lamina (Fig. 1C, D, F). The epidermal cells and the subcuticular space

340 house numerous bacteria (Fig. 1C, D, F). A sub-epithelial nerve plexus is occasionally
341 detectable underneath the basal lamina (Fig. 1E). The cuboidal epidermal cells present
342 different organelles and inclusions (Fig. 1F, G, H) and are connected to each other by apical
343 junctional complexes and to the underlying basal lamina (Fig. 1I) and the dermal layer by
344 hemidesmosomes (Fig. 1J). Secretory cells (granulated cells) are observable (Fig. 1M) all
345 scattered within the epidermis. Presumptive pigment cells (or chromatophores) containing
346 spindle-like electron-dense structures are visible in the dermal layer (Fig. 1C, K, L). These
347 structures, whose specific nature is still unknown, are sometimes present also in the
348 epidermal cells (Fig. 1L).
349
350 ***3.1. Microscopic anatomy of the repair phase***
351 Ben Khadra and co-workers (2015a) provided a general overview of the main events of *E.*
352 *sepositus* repair phase after traumatic arm amputation. Some key concepts are re-called in
353 Fig. S2 (Supplementary Materials) in order to make more immediate the comparison with
354 the repair events of *A. filiformis* reported below.
355
356 *3.1.1. Wound closure*
357 As for starfishes, within few hours p.a. brittle stars respond to injury by limiting coelomic fluid
358 loss and microorganism entrance. However, contrary to the former (Fig. S2A), brittle stars
359 do not form a haemostatic ring but seal the coelomic cavities and vessels (*i.e.* the aboral
360 coelomic cavity and the radial water canal) by bending the first aboral and oral shields
361 proximal to the amputation plane (Fig. 2A). Clotting phenomena of circulating cells (mainly
362 coelomocytes) are immediately visible in the coelomic cavity close to the wound site (Fig.
363 2C) together with the first signs of histolysis and remodelling of injured tissues (mainly
364 muscle bundles) (Fig. 2A).
365 Simultaneously to the first emergency responses, and in agreement with absence of cell
366 proliferation in the first 48 hours p.a. (Czarkwiani *et al.*, 2016), in brittle stars healing of the
367 injury begins with migration of stump epidermal cells. An almost complete wound epidermis,
368 provided with microvilli and cuticle, is visible within 8 hours p.a. (Fig. 2B, 3A). It is composed
369 by a monolayer of slightly elongated epidermal cells characterised by big oval/roundish and
370 patched nucleus and the presence of junctional complexes in their apical portion (Fig. 3B,
371 D). Analysis of serial sections of samples at different regenerative stages suggests that,
372 similarly to starfishes (Fig. S2B), the new epidermis migrates centripetally over the wound.
373 The basal membrane becomes visible only at the middle/late repair phase (after 48-72 hours

374 p.a.), initially as a collection of fragmented pleats and folds rather than a continuous and
375 well-defined layer (Fig. 3H). Increasing number of bacteria are present in the subcuticular
376 layer as well as deep in the wound area at all stages: they are widely spread in the
377 intercellular spaces as well as inside vesicles of the epidermal cells and underlying
378 phagocytes (Fig. 3A, C, F, K). While re-epithelialisation occurs, a layer of different cytotypes
379 (*i.e.* phagocytes and presumptive pigment cells) forms beneath the new epidermis starting
380 at 8 hours p.a. and being visible till 72 hours p.a. (Fig. 2B, 3). During this period, cells of this
381 layer (and of the epidermis) present several cytoplasmic inclusions, such as heterogeneous
382 phagosomes, spindle-shaped electron-dense structures, myelin figures and several types
383 of both electron-lucent and electron-dense inclusions/vesicles (Fig. 3D-G, I-M); these
384 inclusions, together with numerous mitochondria and well-developed rough endoplasmic
385 reticulum (RER), suggest an intense phagocytic and tissue remodelling activity. Junctional
386 complexes do apparently not connect cells which create a thick and compact layer (but not
387 a syncytium) resembling, in position and function, the phagocyte syncytium and the
388 granulation tissue-like observable in starfishes (Fig. S2E; Ben Khadra *et al.*, 2017). Besides
389 the removal of cell debris, this cell layer provides support for the migration of the overlying
390 epidermal cells and acts as cell barrier between the stump tissues and the wound area (Fig.
391 3G). Numerous nervous processes become visible, scattered among this layer, during the
392 middle/late repair phase (48 hours p.a.; Fig. 3J).
393
394 *3.1.2. Collagen appearance*
395 Only after re-epithelialisation and the main remodelling/phagocytosis events are finished,
396 the new extracellular matrix (ECM) is deposited.
397 In starfishes a sparse micro-fibrillar collagenous material is observed from 72 hours p.a. in
398 the oedematous (granulation tissue-like) area (Fig. S2F; Ben Khadra *et al.*, 2017), whereas
399 small bundles of collagen fibrils appear only at the end of the repair phase (one week p.a.;
400 Fig. S2G; Ben Khadra *et al.*, 2017).
401 In brittle stars a comparable oedematous area is never detected. A thin collagenous layer
402 becomes visible below the epidermis starting at 2-3 days p.a. (middle/late repair phase)
403 (Czarkwiani *et al.*, 2016). TEM analyses indicate the absence of organised collagen fibrils
404 till the middle/late repair phase.
405
406 ***3.2. Gene expression in the repair phase***

407 Molecular techniques on adult echinoderms are still not widely established with the
408 expression patterns of the genes here presented being described for the first time. The
409 methods here used are essentially new for starfishes and they provide a new perspective to
410 the study of echinoderm regeneration. Positive and negative controls were performed in
411 both species in order to validate *in situ* hybridisation results. The description of the selected
412 controls and their expression patterns are detailed in the Supplementary Materials (Fig. S5,
413 S6, S7, S8). Here, it is important to stress that the localised expression patterns of the
414 positive controls showed the effectiveness of the techniques in both model systems.
415 Therefore, the analyses of some genes relevant for the repair phase were performed, as
416 detailed below.
417
418 *3.2.1. Immune/inflammatory response-related genes*
419 The precise regulation of the immune response after injury is a critical factor. Therefore, the
420 expression patterns of two relevant genes, known to be involved in human wound healing
421 (Zuliani-Alvarez and Midwood, 2015), were here investigated: a fibrinogen-like (*Ese-fib-like*)
422 for starfishes and a ficolin (*Afi-ficolin*) for brittle stars (Fig. 4). Both proteins contain a
423 fibrinogen-related domain.
424 Fibrinogen is the precursor of fibrin, important for coagulation and granulation tissue
425 formation after wound in vertebrates (Laurens *et al.*, 2006: Drew *et al.*, 2001). A *fibrinogen-*
426 *like* gene, belonging to the FReD superfamily, was isolated in starfishes (see Table S1). The
427 FReD domain was confirmed also using the cDART tool (NCBI). ISH of *Ese-fib-like* shows
428 a distinct staining in the new epithelium covering the wound area at one week p.a. (Fig. 4A)
429 and in the regenerating radial nerve cord in the ectoneural and hyponeural systems at 72
430 hours p.a. (Fig. 4D). In the stump area, *Ese-fib-like* expression is localised in the epidermis
431 (Fig. 4A, B), in the coelomic epithelium lining the perivisceral cavity (Fig. 4B), the papulae
432 (Fig. 4B, C), the radial water canal (Fig. 4E) and the ampullae (Fig. 4F). Free-circulating
433 coelomocytes express also this gene (Fig. 4C) as well as the circular coelomic muscles (Fig.
434 4A).
435 *Ficolins* are considered part of the echinoderm immune gene repertoire (Hibino *et al.*, 2006)
436 as they encode for proteins that are involved in different aspects of innate immunity
437 (Matsushita *et al.*, 2001). A *ficolin* gene, belonging to the FReD superfamily, was isolated in
438 *A. filiformis* (see Table S1). *Afi-ficolin* is expressed in the dermal lining of the epidermis in
439 the regenerative bud at the end of the repair phase (stage 2; Fig. 4H-J). In the stump tissues
440 this transcript is localised in the radial water canal epithelium (Fig. S3).

441

442 *3.2.2. Collagen biosynthesis enzyme gene*

443 Collagen is a key protein of the repair phase and its biosynthesis necessarily needs to be
444 finely regulated. For this reason, the biosynthetic enzyme prolyl-4-hydroxylase (*p4h*;
445 Myllyharju, 2003) was here investigated. The genes of the alpha-1-subunit of *p4h* were
446 identified in both experimental models and their expression patterns analysed during the
447 repair phase.

448 In starfish regenerating tissues *Ese-p4h* expression is detected in the new epidermis at both
449 72 hours and one week p.a. (Fig. 5). The signal in the stump tissues is further described in
450 the Supplementary Materials (Fig. S4A-C) and suggests that other epithelial tissues, such
451 as the coelomic lining and the radial nerve cord, may have a role in collagen biosynthesis.

452 In brittle stars, besides the stump tissues (Fig. S4D), in the regenerative bud *Afi-p4h* is
453 expressed in the coelomic lining but only after the repair phase is finished (Fig. S4E-I).

454

455 ***4. Discussion***

456 In this article we present data on the first events of the regenerative processes in two classes
457 of echinoderms, the Ophiuroidea and the Asteroidea. A comparative approach, with the
458 introduction, for the first time, of molecular and histological analyses, is used, providing us
459 with a new vantage point to understand the high regenerative potential of these systems.
460 The information gathered on the different repair events is discussed below.

461

462 ***4.1. Wound closure***

463 After arm amputation a series of emergency reactions are immediately activated to prevent
464 the loss of body fluids and decrease the wound exposed surface. Differently from *E.*
465 *sepositus* (Ben Khadra *et al.*, 2015a; Ben Khadra *et al.*, 2017) and from starfishes in general
466 (Mladenov *et al.*, 1989; Candia Carnevali *et al.*, 1993; Moss *et al.*, 1998), in brittle stars no
467 evident circular constriction of the arm-tip is detectable. This is consistent with the different
468 brittle star arm anatomy (*i.e.* conspicuous skeletal elements and the absence of a circular
469 muscle layer surrounding the coelomic cavity). Here the apical contraction of the body wall
470 is sufficient for sealing the narrow fluid-filled vessels/cavities (aboral coelomic cavity and
471 radial water canal). In comparison, blood vessel constriction and wound contraction are
472 fundamental events also in mammal wound healing (Pastar *et al.*, 2014; Ibrahim *et al.*, 2015)
473 but while the former is an almost immediate reaction, the latter is delayed comparing to the
474 events happening in both echinoderm models. In humans, skin wound shrinkage slowly

475 starts almost immediately after injury but its main peak of activity occurs around 10 days
476 after the damage (Shultz *et al.*, 2005), different from echinoderms, where it is visible within
477 1-2 days p.a. (Fig. 2A, C). The delay observed in mammals might be due to the "time
478 consuming" activation of fibroblasts resident in the injury's neighbourhood which have to
479 leave their quiescent state, migrate towards the wound and be transformed into
480 myofibroblasts, the ultimate responsible of wound contraction (Martin, 1997).
481 Besides constriction, in both echinoderm species, loss of fluid prevention is also mediated
482 by rapid clotting of circulating cells (coelomocytes), a phenomenon analogous to mammalian
483 platelet clot formation (Peacock, 1984; Clark, 1988; Ibrahim *et al.*, 2015). Noteworthy, in
484 starfishes, coelomocytes displaying platelet-like ultrastructure and function are present
485 (personal observations).
486 Delays or defects in re-epithelialisation can prevent functional wound healing and
487 regeneration (Sivamani *et al.*, 2007). In both *A. filiformis* and *E. sepositus* this step is very
488 rapid though in the former it is accomplished earlier (8-16 hours p.a. *versus* 48-72 hours
489 p.a.), most likely a consequence of the smaller arm size. In mammals, skin re-
490 epithelialisation is accomplished later (around 4 days; Pastar *et al.*, 2014). Noteworthy, in
491 both echinoderm models the new epithelium is formed by elongation of stump epithelial cells
492 present in the adjacent wound edges, without any initial contribution of local proliferation:
493 the onset of cell cycle activity, indeed, occurs far after re-epithelialisation is accomplished
494 (Mladenov *et al.*, 1989; Czarkwiani *et al.*, 2016). Similarly to starfishes (Ben Khadra *et al.*,
495 2015a), in *A. filiformis* regenerating epidermal cells retain their junctional complexes. This
496 common feature of echinoderms markedly distinguishes them from mammals where cell-
497 cell junction disruption is a pre-requisite for migration of keratinocytes over the wound area
498 (Pastar *et al.*, 2014). In both echinoderms and mammals (Clark *et al.*, 1982; Larjava *et al.*,
499 1993) a well-defined basal lamina is not detectable until after the complete differentiation of
500 epidermal cells, which facilitates their migratory movements.
501 The events occurring after re-epithelialisation slightly differ in the histological organisation
502 between the two echinoderm models. Indeed, the wound area of starfish arm is
503 characterised by the presence of a temporary (3-7 days p.a.) oedematous area (Ben Khadra
504 *et al.*, 2015a), not detectable in brittle stars. This area has the aspect of the mammalian
505 granulation tissue and it is characterised by the presence of sparse inflammatory cytotypes
506 (mainly coelomocytes/phagocytes) which can be considered the functional and
507 ultrastructural analogous of monocytes/macrophages (Ryter, 1985; Martin, 1997; Pastar *et*
508 *al.*, 2014). In the outermost part, phagocytes form a continuous syncytial layer underlying

509 the wound epithelium (Ben Khadra *et al.*, 2015a). In brittle stars, a proper oedematous area
510 is lacking, although the compact and persistent phagocyte layer underlying the wound
511 epidermis can be considered, functionally and cytologically, comparable. However, in the
512 latter model cells are separated and never form a syncytium. In both echinoderms the wound
513 is therefore covered by an active and temporary "cellular scar" (*i.e.* a scar mainly composed
514 by cells rather than fibrous matrix), which protects and isolates the delicate underling wound
515 tissues from external insults and pathogens. As for the granulation tissue of mammals, this
516 "tissue" progressively matures in the subsequent days: new cytotypes appear, including
517 nerve elements and presumptive pigment cells, while the ECM is reorganised (see below).
518

519 ***4.2. Immune/inflammatory responses***

520 It is well known that the immune system plays a crucial role during the inflammation phase
521 occurring after injury (Park and Barbul, 2004; MacLeod and Mansbridge, 2015). Two
522 inflammatory/immune response-related genes of echinoderms were here identified: *Ese-fib-*
523 *like* (starfishes) and *Afi-ficolin* (brittle stars).
524 *Ese-fib-like* is a fibrinogen-related (FReD) domain-containing gene. This domain is typical
525 of fibrinogen, the precursor of fibrin in vertebrates. During wound healing fibrin acts as
526 network-forming molecule fundamental for blood coagulation (Laurens *et al.*, 2006) and also
527 for granulation tissue formation and cell migration (Drew *et al.*, 2001). The presence of
528 fibrinogen-like proteins in echinoderms has been described only by Xu and Doolittle (1990)
529 in the sea cucumber *Parastichopus parvimensis* though no expression data is available. The
530 signal detected in the new epidermis and in both the regenerating and the stump coelomic
531 epithelium suggests that these tissues could be involved in the production of fibrinogen-like
532 proteins during the repair phase. Interestingly, the coelomic epithelium is considered one of
533 the "hematopoietic" tissues of echinoderms (Holm *et al.*, 2008), responsible of coelomocytes
534 production, the cells that are involved in clot formation after wound production (see above).
535 However, no clear ultrastructural evidences of fibrin-like network around coelomocyte clot
536 was found. Therefore, deeper investigations are now necessary to understand the functional
537 role of this newly identified fibrinogen-like molecule.
538 In brittle stars *Afi-ficolin* encodes for a protein also containing a FReD domain. In both
539 vertebrates and invertebrates ficolin is a lectin important in the innate immune response
540 (Fujita, 2002; Iwanaga and Lee, 2005; Matsushita, 2009, Zuliani-Alvarez and Midwood,
541 2015). Its presence in the genome/proteome of other echinoderms has been previously
542 reported (Hibino *et al.*, 2006; Franco, 2011). The expression of this transcript at stage 2 in

543 the proximal dermal layer suggests that cells of the new connective tissue may be involved
544 in the immune response after injury. Whether these are new cells or cells recruited from the
545 surrounding stump tissues needs to be further investigated, preferentially through cell
546 tracking. The localised expression in the stump in the radial water canal epithelium suggests
547 that proteins might be synthetized there and subsequently released in the coelomic fluid of
548 the water vascular system, mobilised towards the regenerating area.
549
550 ***4.3. Extracellular matrix deposition and remodelling: a focus on collagen***
551 In line with the general higher speed of regeneration, appearance of an organised fibrous
552 extracellular matrix (ECM) occurs earlier in brittle stars than in starfishes. In both echinoderm
553 models nonfibrillar collagen-like molecules are firstly deposited. However, it is at the end of
554 the repair phase that collagen fibrils and fibril bundles become visible (Fig. S2; Ben Khadra
555 *et al.*, 2015a, b, 2017).
556 To better define collagen production/deposition, the gene expression of a key collagen
557 biosynthetic enzyme (prolyl-4-hydroxylase; *p4h*) was investigated. Till now, few studies have
558 focused on the expression of *p4h* in invertebrates (Veijola *et al.*, 1994; Abrams and Andrew,
559 2002) and in particular in marine invertebrates (Pozzolini *et al.*, 2015). In this context, this
560 study represents a pioneering work. In brittle stars this gene is not apparently expressed in
561 the first phase after injury (it becomes visible only at advanced stages in the coelomic
562 epithelium), whereas in starfishes it is localised in the regenerating epidermis at the
563 middle/late repair phase, supporting a role of this tissue in early collagen
564 biosynthesis/deposition. For *A. filiformis* the apparent incongruences between the absence
565 of *Afi-p4h* expression till the onset of the regenerative phase and the microscopic detection
566 of collagen from the end of the repair phase need to be further investigated through
567 quantitative PCR (also at earlier stages).
568 Noteworthy, in both echinoderms ECM deposition starts later than in mammals (Clore *et al.*,
569 1979): indeed, in the latter new collagen appears at the very beginning of the repair phase
570 (from about 10 hours after injury). A reticular and disorganised fibrillar network of collagen
571 type III is firstly deposed and then replaced by thick, dense and parallel fibres of collagen
572 type I that are constantly remodelled (Xue and Jackson, 2015). Differently, in echinoderms
573 collagen deposition begins only at the end of the repair phase and it initially occurs as non-
574 fibrillar loose ECM, possibly providing a more “dynamic and plastic” environment for tissue
575 regeneration. Moreover, as already suggested for sea cucumbers (Quiñones *et al.*, 2002)

576 and contrary to mammals (Bock and Mrowietz, 2002; Rahban and Garner, 2003), in both
577 brittle stars and starfishes no fibrotic scar is normally detected.
578
579 ***4.4. Conclusions***
580 In this study the brittle star *Amphiura filiformis* and the starfish *Echinaster sepositus* were
581 used as models to describe and compare the repair phase phenomena after arm amputation
582 within echinoderms as well as with mammals' healing events after wound. The main
583 similarities and differences between them are summarised in Table 1 and Fig. 6.
584 Taken together, our results show that:
585 • both echinoderm models display similar haemostasis, wound contraction and re-
586 epithelialisation phenomena and, in comparison to mammals, they are overall more
587 efficient during the emergency reaction after injury in terms of timing and efficacy;
588 • the regenerating epidermis of echinoderms is apparently a highly active and multi-
589 functional tissue, involved in both inflammatory/immune response (phagocytosis),
590 plus in collagen biosynthesis;
591 • the extracellular matrix (ECM) fibrillar organisation after injury is comparable in the
592 two echinoderm models and it is delayed and less conspicuous than in mammals.
593 Moreover, over-deposition of collagen (fibrosis) is never detectable. Overall, the
594 temporary loose configuration of the ECM is likely to be more "plastic" than the
595 collagenous scar of mammals, therefore possibly facilitating the subsequent
596 regenerative process, as suggested for sea cucumbers (Quiñones *et al.*, 2002).
597 It is important to point out that re-epithelialisation, inflammatory/immune system-related
598 genes and ECM fibrillar organisation/deposition during brittle star and starfish repair phases
599 were here deeply described. Furthermore, interesting differences and similarities in repair
600 events and timing within echinoderms and between echinoderms and mammals were
601 highlighted. The comparison between animals able or unable to regenerate after injury
602 suggests that regenerative abilities are mechanistically diverse, from the very first repair
603 events. These differences, contrary to what is assumed, are not just differences in the
604 subsequent re-growth capacities. In the future, perturbation tests aimed to impair/block re-
605 epithelialisation, immune response or ECM deposition should be performed to test the
606 hypothesis that specific repair events are strictly necessary to permit an efficient
607 regenerative process. Moreover, our findings show that echinoderms, and starfishes
608 especially, can be considered valid alternative models to study wound healing and
609 regeneration in light of human health future applications (Gurtner *et al.*, 2008).

610

611 **Table 1.** *Comparison of the events occurring during the repair phase of echinoderms and*
612 *mammals.* Symbol: * - data from Martin, 1997; Werner and Grose, 2003; Pastar *et al.*, 2014.
613

| EVENT | STARFISHES | BRITTLE STARS | MAMMALS* |
|---|---|---|---|
| **Constriction of the cavities/canals** | Sealing of the coelomic cavities (haemostatic ring) | Sealing of the coelomic cavities (no haemostatic ring, bending of the shields) | Vasoconstriction of the blood vessels |
| **Wound contraction** | Aboral body wall moves towards the oral side (within 24 hours p.a.) | Aboral and oral body walls move towards the wound (within 24 hours p.a.) | Contraction of the wound edges (after 3-4 days post injury) |
| **Cell clotting in the cavities/canals** | Coelomocytes | Coelomocytes | Platelets |
| **Phagocytosis** | Phagocytes/ coelomocytes | Phagocytes/coelomocytes/ epidermis | Macrophages |
| **Re-epithelialisation direction** | Centripetal | Centripetal | Centripetal |
| **Epidermal cell junction disruption** | No | No | Yes |
| **Oedematous area (granulation tissue-like) formation** | Yes | No | Granulation tissue |
| **Canal/vasa infiltration** | No | No | Yes (angiogenesis) |
| **Fibrosis** | No | No | Yes |

614

615 **Acknowledgements**

616 The authors thank the Sven Lovén Centre for Marine Sciences in Kristineberg (Sweden),
617 especially Sam Dupont and Bengt Lundve, for the collection of experimental brittle stars and
618 the Marine Protected Areas of Portofino and Bergeggi Island (Ligurian Sea, Italy) for the
619 permission to collect experimental starfishes. A special thanks to the SCUBA divers Marco
620 Benati, Marco Di Lorenzo and Paola Fasano for starfish collection. We thank Prof. Max
621 Telford, Fraser Simpson and Wendy Hart for help with gene cloning, Dr. Avi Lerner for
622 providing *ets1/2* degenerate primers, Laura Piovani and Mark Turmaine for help with
623 transmission electron microscopy protocols.

624

625 **Conflict of interest disclosure**

626 The authors certify that there is no conflict of interest. All authors contributed to and
627 approved the final manuscript.

628

629 **Authors' contributions and funding**

CF, PO and MS conceived the study. CF, AC, AZ, YBK, GC carried out the experiments. YBK and PM provided the sequence of *Ese-actin*. CF, AC, FB, MS, PO and MDCC analysed the data. CF, PO, PM and MS wrote the manuscript. This work was partly funded by the KVA fund SL2015-0048 from the Royal Swedish Academy of Science. CF was funded by an Erasmus Placement Fellowship. AC was funded by a Wellcome Trust PhD studentship. MS was funded by a Young Researcher Grant of the University of Milan.

## References

Abrams EW and Andrew DJ. Prolyl 4-hydroxylase alpha-related proteins in *Drosophila melanogaster*: tissue-specific embryonic expression of the 99F8-9 cluster. Mech Dev 2012, 112:165-171.

Akimenko MA, Marì-Beffa M, Becerra J, Géraudie J. Old Questions, New Tools, and Some Answers to the Mystery of Fin Regeneration. Developmental Dynamics 2003, 226:190-201.

Arnone MI, Byrne M, Martinez P. Echinodermata. In: Evolutionary Developmental Biology of Invertebrates. Vol 6 (Deuterostomia) 2015, A. Wanninger (ed.), DOI: 10.1007/978-3-7091-1856-6_1, Springer-Verlag Wien.

Bateman PW and Fleming PA. To cut a long tail short: a review of lizard caudal autotomy studies carried out over the last 20 years. Journal of Zoology 2009, 277:1-14.

Bely AE. Distribution of segment regeneration ability in the Annelida. Integr Comp Biol 2006, 46:508-518.

Ben Amar M and Bianca C. Towards a unified approach in the modeling of fibrosis: A review with research perspectives. Physics of Life Reviews 2016, 17:61-85.

Ben Khadra Y, Ferrario C, Di Benedetto C, Said K, Bonasoro F, Candia Carnevali MD, Sugni M. Wound repair during arm regeneration in the red starfish *Echinaster sepositus*. Wound Repair Regen 2015a, 23:611-622.

Ben Khadra Y, Ferrario C, Di Benedetto C, Said K, Bonasoro F, Candia Carnevali MD, Sugni M. Re-growth, morphogenesis, and differentiation during starfish arm regeneration. Wound Repair Regen 2015b, 23:623-634.

Ben Khadra Y, Sugni M, Ferrario C, Bonasoro F, Varela Coelho A, Martinez P, Candia Carnevali MD. An integrated view of asteroid regeneration: tissues, cells and molecules. Cell and Tissue Research 2017, DOI: 10.1007/s00441-017-2589-9.

Biressi A, Ting Z, Dupont S, Dahlberg C, Di Benedetto C, Bonasoro F, Thorndyke M, Candia Carnevali MD. Wound-healing and arm regeneration in *Ophioderma longicaudum* and *Amphiura filiformis* (Ophiuroidea, Echinodermata): comparative morphogenesis and histogenesis. Zoomorphology 2010, 129:1-19.

Bock O and Mrowietz U. Keloids. A fibroproliferative disorder of unknown etiology. Hautarzt 2002, 53: 515.

Bosch TCG. Why polyps regenerate and we don't: Towards a cellular and molecular framework for *Hydra* regeneration. Developmental Biology 2007, 303:421-433.

669 Brockes JP and Kumar A. Plasticity and reprogramming of differentiated cells in amphibian
670 regeneration. Molecular Cell Biology 2002, 3:566-574.

671 Cabrera-Serrano A and García-Arrarás JE. RGD-containing peptides inhibit regeneration in
672 the sea cucumber *Holothuria glaberrima*. Dev Dyn 2004, 231:171-178.

673 Candia Carnevali MD. Regeneration in echinoderms: repair, regrowth, cloning. ISJ 2006,
674 3:64-76.

675 Candia Carnevali MD and Bonasoro F. A microscopic overview of crinoid regeneration.
676 Microsc Res Techniq 2001, 55:403-426.

677 Candia Carnevali MD, Lucca E, Bonasoro F. Mechanisms of arm regeneration in the feather
678 star *Antedon mediterranea*: healing of wound and early stages of development. The Journal
679 of Experimental Zoology 1993, 267:299-317.

680 Clark RA. Overview and general considerations of wound repair. In: Clark RAF, Henson PM
681 (eds) The molecular and cellular biology of wound repair. Plenum, New York, 1988, 3-23.

682 Clark RAF, Lanigan JM, DellaPelle P, Manseau E, Dvorak HF, Colvin RB. Fibronectin and
683 Fibrin Provide a Provisional Matrix for Epidermal Cell Migration During Wound
684 Reepithelialization. The Journal of Investigative Dermatology 1982, 79:264-269.

685 Clore JN, Cohen IK, Diegelmann RF. Quantitation of Collagen Types I and III during Wound
686 Healing in Rat Skin. Experimental Biology and Medicine 1979, 161.

687 Czarkwiani A, Dylus DV, Oliveri P. Expression of skeletogenic genes during arm
688 regeneration in the brittle star *Amphiura filiformis*. Gene Expression Patterns 2013, 13:464-
689 472.

690 Czarkwiani A, Ferrario C, Dylus DV, Sugni M, Oliveri P. Skeletal regeneration in the brittle
691 star *Amphiura filiformis*. Frontiers in Zoology 2016, 13:18.

692 Diegelmann RF and Evans MC. Wound healing: an overview of acute, fibrotic and delayed
693 healing. Frontiers in Bioscience 2004, 9:283-289.

694 Drew AF, Liu H, Davidson JM, Daugherty CC, Degen JL. Wound-healing defects in mice
695 lacking fibrinogen. Blood 2001, 97:3691-3698.

696 Ducati CC, Candia Carnevali MD, Barker MF. Regenerative potential and fissiparity in the
697 starfish *Coscinasterias muricata*. Echinoderms: Munchen: Proceedings of the 11th
698 International Echinoderm Conference, 6-10 October 2003, Munich, Germany. 50:112-118.
699 CRC Press 2004.
700

701 Dupont S and Thorndyke MC. Growth or differentiation? Adaptive regeneration in the brittle
702 star *Amphiura filiformis*. The Journal of Experimental Biology 2006, 209:3873-3881.
703

704 Dylus DV, Blowes LM, Czarkwiani A, Elphick MR, Oliveri P. Developmental transcriptome
705 of the brittlestar *Amphiura filiformis* reveals gene regulatory network rewiring in echinoderm
706 larval skeleton evolution." BioRxiv 2017, DOI: 10.1101/166991.
707

708 Etchevers HC, Vincent C, Le Douarin NM, Couly GF. The cephalic neural crest provides
709 pericytes and smooth muscle cells to all blood vessels of the face and forebrain.
710 Development 2001, 128:1059-1068.
711

712 Franco CDMF. Proteomics based approach to understand tissue regeneration. Starfish as
713 a model organism. PhD thesis 2011.
714
715 Fujita T. Evolution of the lectin-complement pathway and its role in innate immunity. Nature
716 Reviews 2002, 2:346-353.
717
718 Gillis JA, Modrell MS, Northcutt RG, Catania KC, Luer C, Baker CVH. Electrosensory
719 ampullary organs are derived from lateral line placodes in cartilaginous fishes. Development
720 2012, 139:3142-3146.

721 Guo S and DiPietro LA. Factors affecting wound healing. J Dent Res 2010, 89:219-229.

722 Gurtner GC, Werner S, Barrandon Y, Longaker MT. Wound repair and regeneration. Europe
723 PMC 2008, 453:314-321.

724 Hibino T, Loza-Coll M, Messier C, Majeske AJ, Cohen AH, Terwilliger DP, Buckley KM,
725 Brockton V, Nair SV, Berney K, Fugmann SD, Anderson MK, Pancer Z, Cameron RA, Smith
726 LC, Rast JP. The immune gene repertoire encoded in the purple sea urchin genome.
727 Developmental Biology 2006, 300:349-365.

728 Holm K, Dupont S, Sköld HN, Stenius A, Thorndyke MC, Hernroth B. Induced cell
729 proliferation in putative haematopoietic tissues of the sea star, *Asterias rubens* (L.). J Exp
730 Biol 2008, 211:2551-2558.

731 Hyman LH. The Invertebrates. Vol. 4. Echinodermata. Mc Graw Hill Book Company Inc.
732 New York, Toronto, London, 1955.

733 Ibrahim MM, Chen L, Bond JE, Medina MA, Ren L, Kokosis G, Selim AM and Levinson H.
734 Myofibroblasts contribute to but are not necessary for wound contraction. Laboratory
735 Investigation 2015, 95:1429-1438.

736 Iwanaga S and Lee BL. Recent Advances in the Innate Immunity of Invertebrate Animals.
737 Journal of Biochemistry and Molecular Biology 2005, 38:128-150.

738 Larjava H, Salo T, Haapasalmi K, Kramer RH, Heino J. Expression of Integrins and
739 Basement Membrane Components by Wound Keratinocytes. J Clin Invest 1993, 92:1425-
740 1435.

741 Laurens N, Koolwijk P, De Maat PM. Fibrin structure and wound healing. Journal of
742 Thrombosis and Haemostasis 2006, 4:932-939.

743 MacLeod AS and Mansbridge JN. The Innate Immune System in Acute and Chronic
744 Wounds. Advances in Wound Care Mary Ann Liebert, Inc. 2015, 5:65-78.

745 Martin P. Wound healing-aiming for perfect skin regeneration. Science 1997, 276:75-81.

746 Mashanov VS and García-Arrarás JE. Gut Regeneration in Holothurians: A Snapshot of
747 Recent Developments. The biological bulletin 2011, 221:93-109.

748 Matsushita M. Ficolins: Complement-Activating Lectins Involved in Innate Immunity. J Innate
749 Immun 2009, 2:24-32.

750 Mladenov PV, Bisgrove B, Asotra S, Burke RD. Mechanisms of arm-tip regeneration in the
751 sea star, *Leptasterias hexactis*. Roux's Arch Dev Biol 1989, 198:19-28.

752 Moss C, Hunter J, Thorndyke MC. Pattern of bromodeoxyuridine incorporation and
753 neuropeptide immunoreactivity during arm regeneration in the starfish *Asterias rubens*. Phil
754 Trans R Soc London B 1998, 353:421-436.

755 Mozzi D, Dolmatov IY, Bonasoro F, Candia Carnevali MD. Visceral regeneration in the
756 crinoid *Antedon mediterranea*: basic mechanisms, tissues and cells involved in gut regrowth.
757 Cent Eur J Biol 2006, 1:609-635.

758 Myllyharju J. Prolyl 4-hydroxylases, the key enzymes of collagen biosynthesis. Matrix
759 Biology 2003, 22:15-24.

760 Oji T. Fossil records of echinoderm regeneration with special regard to crinoids. Micr Res
761 Tech 2001, 55:397-402.

762 Pancer Z, Rast JP, Davidson EH. Origins of immunity: transcription factors and homologues
763 of effector genes of the vertebrate immune system expressed in sea urchin coelomocytes.
764 Immunogenetics 1999, 49:773-86.

765 Park JE and Barbul A. Understanding the role of immune regulation in wound healing. The
766 American Journal of Surgery 2004, 187:11S-16S.

767 Pastar I, Stojadinovic O, Yin NC, Ramirez H, Nusbaum AG, Sawaya A, Patel SB, Khalid L,
768 Isseroff RR, Tomic-Canic M. Epithelialization in Wound Healing: A Comprehensive Review.
769 Adv Wound Care (New Rochelle) 2014, 3:445-464.

770 Peacock EE. Wound repair. In: Wound repair. Saunders, Philadelphia 1984, 38-55.

771 Pozzolini M, Scarfì S, Mussino F, Ferrando S, Gallus L, Giovine M. Molecular Cloning,
772 Characterization, and Expression Analysis of a Prolyl 4-Hydroxylase from the Marine
773 Sponge *Chondrosia reniformis*. Mar Biotechnol 2015, 17:393-407.

774 Quiñones JL, Rosa R, Ruiz DL, García-Arrarás JE. Extracellular matrix remodelling and
775 metalloproteinase involvement during intestine regeneration in the sea cucumber *Holothuria*
776 *glaberrima*. Dev Biol 2002, 250:181-197.

777 Rahban SR and Garner WL. Fibroproliferative scars. Clin Plast Surg 2003, 30:77.

778 Ramírez-Gómez F, Ortiz-Pineda PA, Rojas Cartagena C, Suarez-Castillo EC, García-
779 Arrarás JE. Immune-related genes associated with intestinal tissue in the sea cucumber
780 *Holothuria glaberrima*. Immunogenetics 2008, 60:57-71.

781 Ramírez-Gómez F, Ortiz-Pineda PA, Rivera Cardona G, García-Arrarás JE. LPS-induced
782 genes in intestinal tissue of the sea cucumber *Holothuria glaberrima*. PLoS ONE 2009,
783 4:e6178.

784 Ramírez-Gómez, F, Aponte-Rivera F, Mendez Castaner L, García-Arrarás JE. Changes in
785 holothurian coelomocyte populations following immune stimulation with different molecular
786 patterns. Fish Shellfish Immunol 2010, 29:175-185.

787 Ramírez-Gómez F and García-Arrarás JE. Echinoderm immunity. ISJ 2010, 7:211-220.

788 Rast JP, Smith LC, Loza-Coll M, Hibino T, Litman GW. Genomic Insights into the Immune
789 System of the Sea Urchin. Science 2006, 314:952-956.

790 Ryter A. Relationship between ultrastructure and specific functions of macrophages.
791 Comparative Immunology, Microbiology and Infectious Diseases 1985, 8:119-133.

Saló E, Abril JF, Adell T, Cebrià F, Eckelt K, Fernàndez-Taboada E, Handberg-Thorsager M, Iglesias M, Molina MD, Rodrìguez-Esteban G. Planarian regeneration: achievements and future directions after 20 years of research. Int J Dev Biol 2009, 53:1317-1327.

Sánchez Alvarado A. Regeneration in the metazoans: why does it happen? BioEssays 2000, 22:578-590.

Shultz GS, Ladwig G, Wysocki A. Extracellular matrix: review of its roles in acute and chronic wounds. World Wide Wounds 2005.

Singer AJ and Clark RAF. Cutaneous wound healing. The New England Journal of Medicine 1999, 341:738-746.

Sivamani RK, Garcia MS, Isseroff RR. Wound re-epithelialization: modulating keratinocyte migration in wound healing. Front Biosci 2007, 12:2849-2868.

Smith LC, Ghosh C, Buckley KM, Clow LA, Dheilly NM, Haug T, Henson JH, Li C, Lun CM, Majeske AJ, Matranga V, Nair SV, Rast JP, Raftos DA, Roth M, Sacchi S, Schrankel CS, Stensvåg K. Echinoderm immunity. Invertebrate Immunity, edited by Kenneth Söderhäll © 2010 Landes Bioscience and Springer Science+Business Media.

Stroncek JD and Reichert WM. Overview of Wound Healing in Different Tissue Types. In: Reichert WM, editor. Indwelling Neural Implants: Strategies for Contending with the *In Vivo* Environment. Boca Raton (FL): CRC Press/Taylor & Francis 2008, Chapter 1.

Tredget EF, Nedelec B, Scott PG, Ghahary A. Hypertrophic scars, keloids and contractures: the cellular and molecular basis for therapy. Surg Clin North Am 1997, 77:701-730.

Veijola J, Koivunen P, Annunen P, Pihlajaniemi T, Kivirikko KI. Cloning, baculovirus expression, and characterization of the alpha subunit of prolyl 4-hydroxylase from the nematode *Caenorhabditis elegans*. This alpha subunit forms an active alpha beta dimer with the human protein disulfide isomerase/beta subunit. J Biol Chem 1994, 269:26746-26753.

Werner S and Grose R. Regulation of wound healing by growth factors and cytokines. Physiol Rev 2003, 83:835.

White LM, Roy S, Gordillo GM, Kalliainen LK, Melvin WS, Ellison EC, Sen CK. Wound healing and regeneration. Physiology and Maintenance 2009, Volume 1.

Xu X and Doolittle RF. Presence of a vertebrate fibrinogen-like sequence in an echinoderm. Proc Natl Acad Sci USA 1990, 87:2097-2101.

Xue M and Jackson CJ. Extracellular Matrix Reorganization During Wound Healing and Its Impact on Abnormal Scarring. Advances in Wound Care 2015, 4:119-136.

Zhang G and Cohn MJ. Hagfish and lancelet fibrillar collagens reveal that type II collagen-based cartilage evolved in stem vertebrates. PNAS 2006, 103:16829-16833.

Zuliani-Alvarez L and Midwood KS. Fibrinogen-Related Proteins in Tissue Repair: How a Unique Domain with a Common Structure Controls Diverse Aspects of Wound Healing. Advances in Wound Care 2015, 4:273-285.

**Captions of the figures of the main text**

832 **Fig. 1.** *Ultrastructure of the brittle star stump (non-regenerating) epidermis*. Light microscopy
833 (LM) and transmission electron microscopy (TEM). A) Semi-thin sagittal section of the aboral
834 epidermis (arrowhead). B) Semi-thin sagittal section of the oral epidermis (arrowhead). C)
835 The aboral epidermis shows the cuboid epidermal cells nested in the skeletal trabeculae
836 and covered by a well-defined cuticle (arrowhead). The subcuticular space hosts numerous
837 bacteria (asterisks) and beneath the epidermis a presumptive pigment cell is visible (arrow).
838 D) In the oral epidermis bacteria are visible in the subcuticular space (asterisk) and the
839 pleats and folds of the basal lamina (arrow) are present immediately beneath the epidermal
840 cells. E) Detail of Fig. D showing the pleats and folds of the basal lamina and the presence
841 of scattered nervous processes (arrowhead). F) The epidermal cells show microvilli
842 branching in the subcuticular space (arrowheads) and a bacterium inside the cell and
843 surrounded by a membrane (asterisk). G) Detail of Fig. F showing the abundant apical Golgi
844 apparatus (arrows). H) Inclusions of different types (arrows), electron-lucent vesicles
845 (asterisks) and abundant RER (arrowhead) are visible in the epidermal cells. I) The basal
846 lamina shows both thin (white arrowhead) and thick (black arrowhead) structure. Thin
847 collagen fibrils are present immediately underneath. J) In the apical portion of the epidermis
848 the apical zonulae (white arrowhead) and subjacent septate junction (black arrowhead) are
849 visible between two adjacent epidermal cells. Hemidesmosomes (arrows) are connecting
850 the epidermal cells with the underlying basal lamina (asterisk) to maintain epidermis
851 integrity. K) In the presumptive pigment cells the spindle-like electron-dense structures
852 (arrowheads) are present both surrounded or not by a thin membrane. L) The aboral
853 epidermis shows a big presumptive pigment cell underneath the epidermis. Spindle-shaped
854 electron-dense structures (asterisks) are spread in the cytoplasm and are present in lower
855 amount also in some epidermal cells. M) A presumptive secretory cell is scattered among
856 epidermal cells showing long microvilli in the subcuticular space apically breaking the cuticle
857 (arrowhead) and compact electron-dense material packed in roundish membrane-bound
858 vesicles (asterisk) in the cytoplasm. Junction complexes connect this cells to the adjacent
859 epidermal cells. Abbreviations and symbols: acc - aboral coelomic cavity; bl - basal lamina;
860 c - collagen fibril; m in A - muscle; m in J - mitochondrion; n in B - radial nerve cord; n in H -
861 nucleus; t - trabecula; asterisk in C, D, F - bacteria; asterisk in J - basal lamina; asterisk in
862 H - electron-lucent vesicle; asterisk in L - spindle-shaped electron-dense structure; asterisk
863 in M - electron-dense granule.
864

865 **Fig. 2.** *Main events of A. filiformis repair phase*. Light microscopy (LM). A) Semi-thin
866 parasagittal section showing the downward and upward movements of the aboral shield and
867 of the oral shield respectively (arrows) to help wound closure. The intervertebral muscles
868 involved in the amputation already show rearrangement phenomena (arrowhead). B) Semi-
869 thin sagittal section where the new epithelium covers the whole wound surface (arrow) and
870 the main body cavities (aboral coelomic cavity and radial water canal) are already sealed.
871 C) Semi-thin sagittal section showing that cells (possibly coelomocytes) are clotting in the
872 aboral coelomic cavity lumen in order to seal it and avoid loss of fluid (arrow). Abbreviations
873 and symbols: acc - aboral coelomic cavity; m - muscle; n - radial nerve cord; p - podium; rwc
874 - radial water canal.
875
876 **Fig. 3.** *Main events of the A. filiformis repair phase*. Transmission electron microscopy
877 (TEM). A) The new epithelium presents cells with an oval/roundish nucleus and well-defined
878 nucleolus. The cuticle is already observable (arrowhead) and numerous bacteria (arrows)
879 are present both underneath the epithelium and in the subcuticular space. B) Detail of an
880 apical junction complex (arrow) between adjacent cells of the new epithelium. C) Detail of
881 bacteria enveloped by a thin membrane. D) New epithelial cells show a well-defined cuticle
882 (arrowhead) and patchy nuclei; several phagosomes are detectable. E) Detail of D on
883 phagosomes. F) The new epidermis presents elongated epidermal cells and a well-defined
884 cuticle. Numerous phagosomes (arrowheads) and mitochondria (asterisk) are visible in both
885 epidermal cells and in the underneath thick layer of cells. G) Different cytotypes are present
886 beneath the new epidermis and create a layer dividing the rearranging/regenerating area
887 from the stump extracellular matrix mainly composed of collagen fibrils. H) The new basal
888 lamina (arrowhead) is visible as pleats and folds beneath the epidermal cells. I) Different
889 cytotypes are observable underneath the new epidermis: cells do not form a syncytium and
890 present abundant RER, phagosomes (arrowhead), spindle-shaped electron-dense
891 structures (arrow) and numerous mitochondria. J) Numerous nervous processes
892 (arrowheads) with mitochondria are visible scattered among the different cytotypes. K) In
893 the regenerating area new epidermal cells present a flat-cubic shape and the rearranging
894 contractile apparatus of several myocytes (arrows) is phagocytised by cells underneath the
895 new epidermis. L) In the rearranging/regenerating area spindle-shaped electron-dense
896 structures (arrowhead) are visible together with myofilaments (asterisk). Myelin figures are
897 present as well (arrow). M) The rearranging contractile apparatus of a myocyte (arrow)
898 inside the phagosome of a cell underneath the new epidermis. Abbreviations and symbols:

c - collagen; m - mitochondrion; n - nucleus; RER - rough endoplasmic reticulum; asterisk in F - mitochondria; asterisk in L - myosin filaments.

**Fig. 4.** *Expression pattern of Ese-fib-like on E. sepositus regenerating arms (A-G) and of Afi-ficolin on A. filiformis regenerating arms (H-J).* A) *Ese-fib-like* is expressed in the new epidermis (orange arrowhead), in the circular coelomic muscles (black arrowhead) and in the epidermis of the stump (arrow). B) In the stump expression is detectable in the coelomic epithelium (arrowhead), in the coelomic lining of the papulae (arrows) but no signal is present in the mucous gland (asterisk). C) Cells in the papulae (possibly coelomocytes) are stained (arrow). D) The regenerating radial nerve cord is stained in both ectoneural (arrowhead) and hyponeural (arrow) systems. E) *Ese-fib-like* is expressed at the level of the radial water canal epithelium (arrow) of the stump. F) The inner lining of the stump ampullae (arrowhead) expresses this transcript. G) Sagittal section scheme where black boxes indicate corresponding images of this figure to facilitate the understanding of the expression pattern location. H) WMISH sample showing that *Afi-ficolin* is expressed in the dermal layer below the epidermis (arrowhead). I) Post *in situ* paraffin section showing the expression of *Afi-ficolin* in the dermal layer of the regenerative bud (arrowheads). J) Sagittal section scheme showing *Afi-ficolin* expression pattern in the regenerative bud. Signal is highlighted in violet. Red dotted lines: amputation plane. Abbreviations and symbols: AV - aboral view; c - coelom; ct - connective tissue; e - epidermis; m - muscle; o - ossicle; p - podium; SS - sagittal section; asterisk - mucous gland.

**Fig. 5.** *Expression pattern of Ese-p4h on E. sepositus regenerating arms.* A) In a 72 hours p.a. sample *Ese-p4h* is expressed in the regenerating epidermis (dotted square) and in the epidermis of the stump (arrowhead). B) Detail of A on the signal in the regenerating epidermis (arrow). C) The new epidermis at one week p.a. shows a signal (arrow). D) Sagittal section scheme where black boxes indicate corresponding images of this figure to facilitate the understanding of the expression pattern location. Red dotted line: amputation plane. Abbreviations: ct - connective tissue; m - muscle; p - podium.

**Fig. 6.** *Main similarities/differences in the events of the repair phase among starfishes (E. sepositus), brittle stars (A. filiformis) and mammals*. See colour legend embedded in the figure.

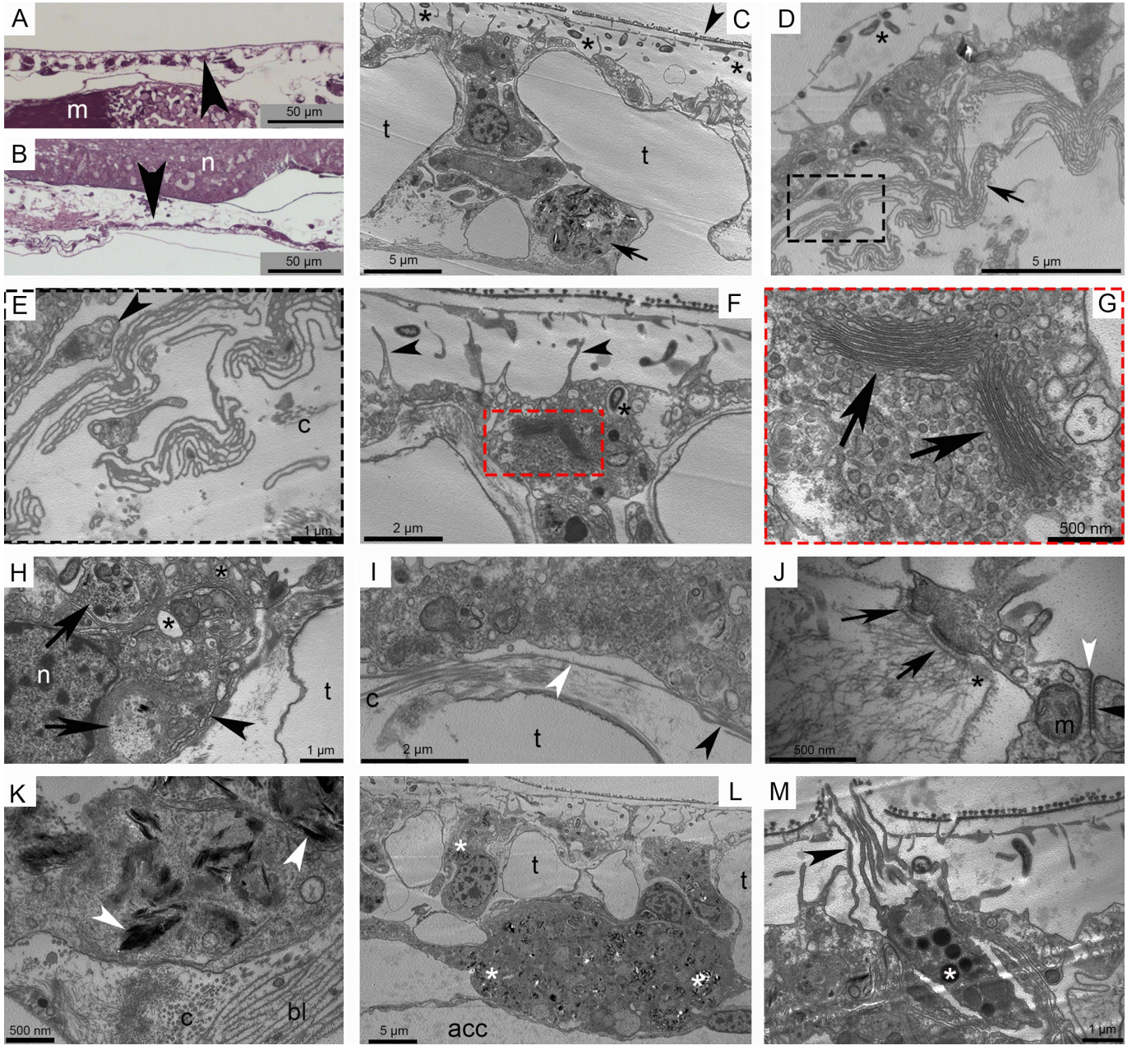
A
m
50 µm
B
n
50 µm
C
t
t
5 µm
D
5 µm
E
c
1 µm
F
2 µm
G
500 nm
H
n
t
1 µm
I
c
t
2 µm
J
m
500 nm
K
c
bl
500 nm
L
t
t
acc
5 µm
M
1 µm

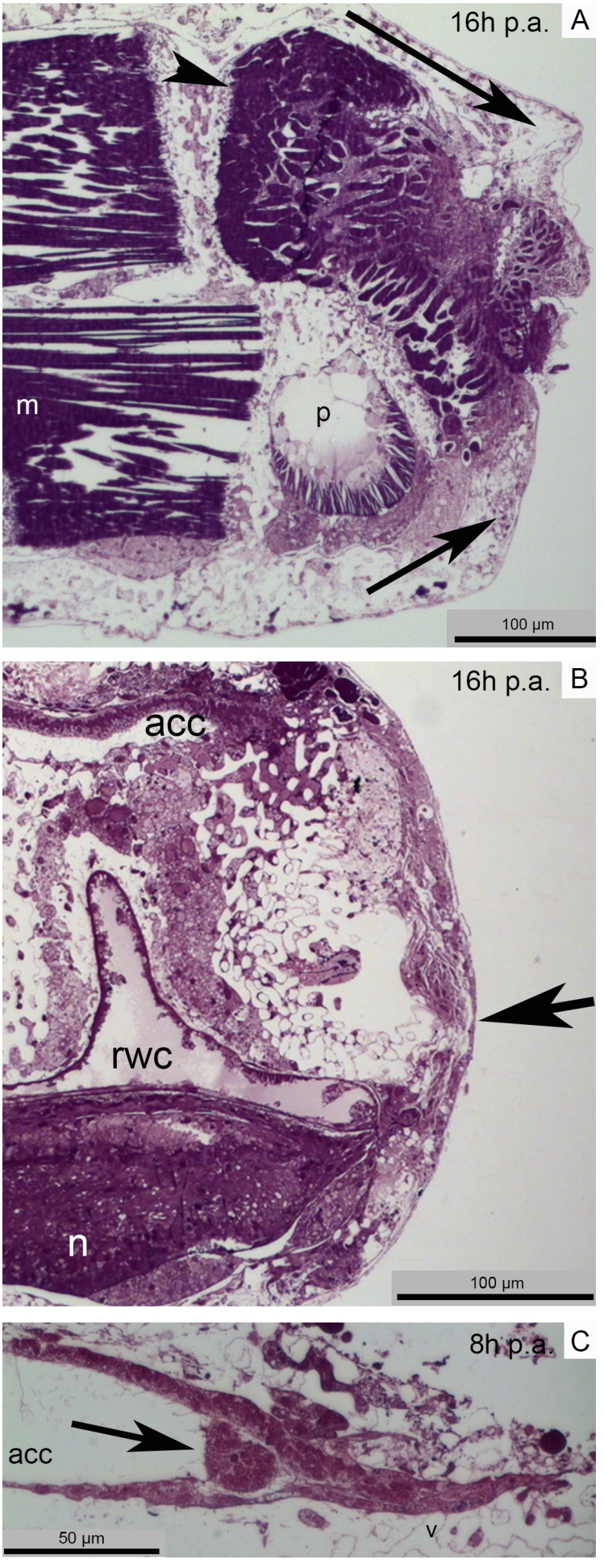
16h p.a.
A
m
p
100 µm
16h p.a.
B
acc
rwc
n
100 µm
8h p.a.
C
acc
v
50 µm

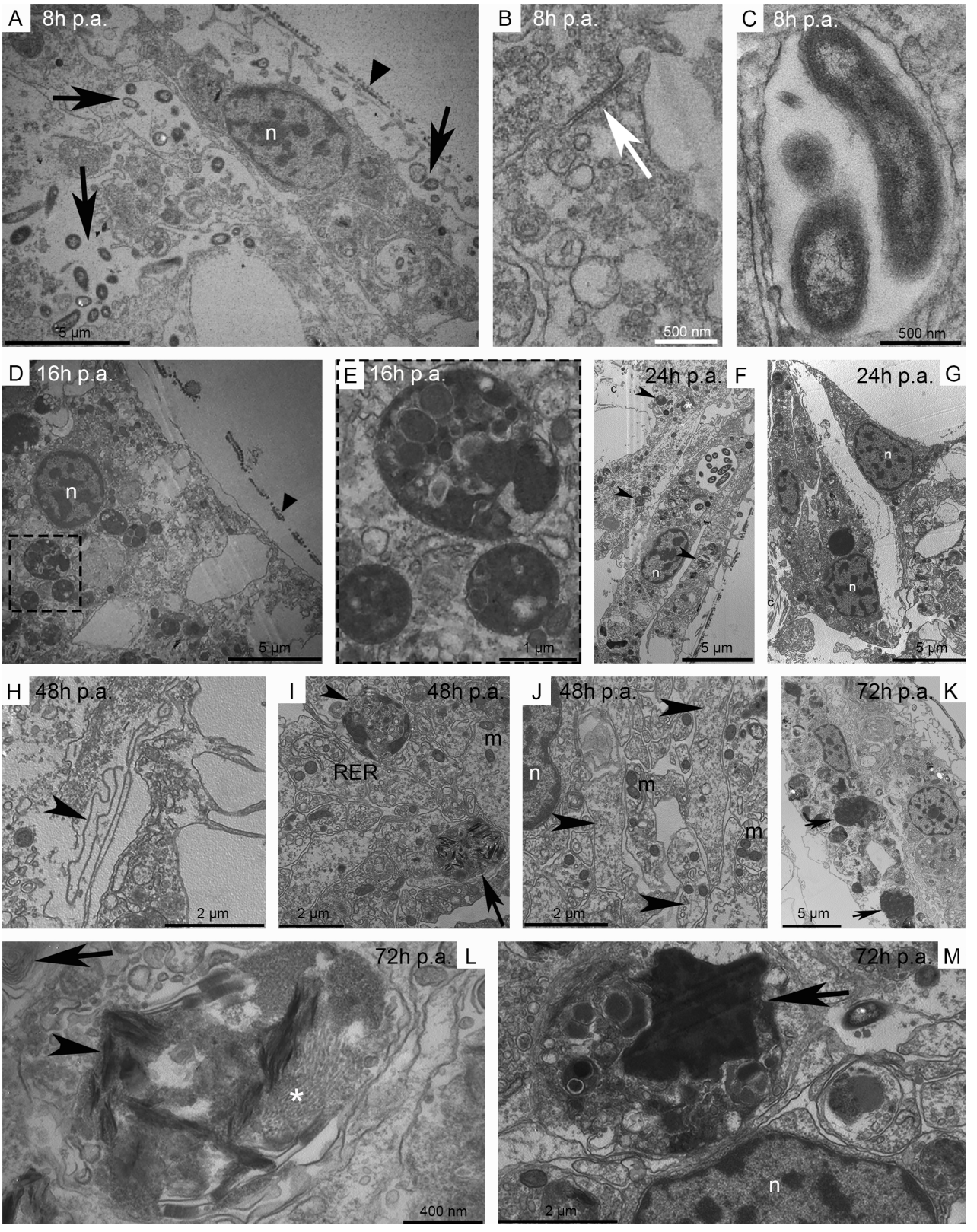
A 8h p.a.
n
5 µm
B 8h p.a.
500 nm
C 8h p.a.
500 nm
D 16h p.a.
n
5 µm
E 16h p.a.
1 µm
24h p.a. F
c
n
5 µm
24h p.a. G
n
n
c
5 µm
H 48h p.a.
2 µm
I 48h p.a.
m
RER
2 µm
J 48h p.a.
n
m
m
2 µm
72h p.a. K
5 µm
72h p.a. L
*
400 nm
72h p.a. M
n
2 µm

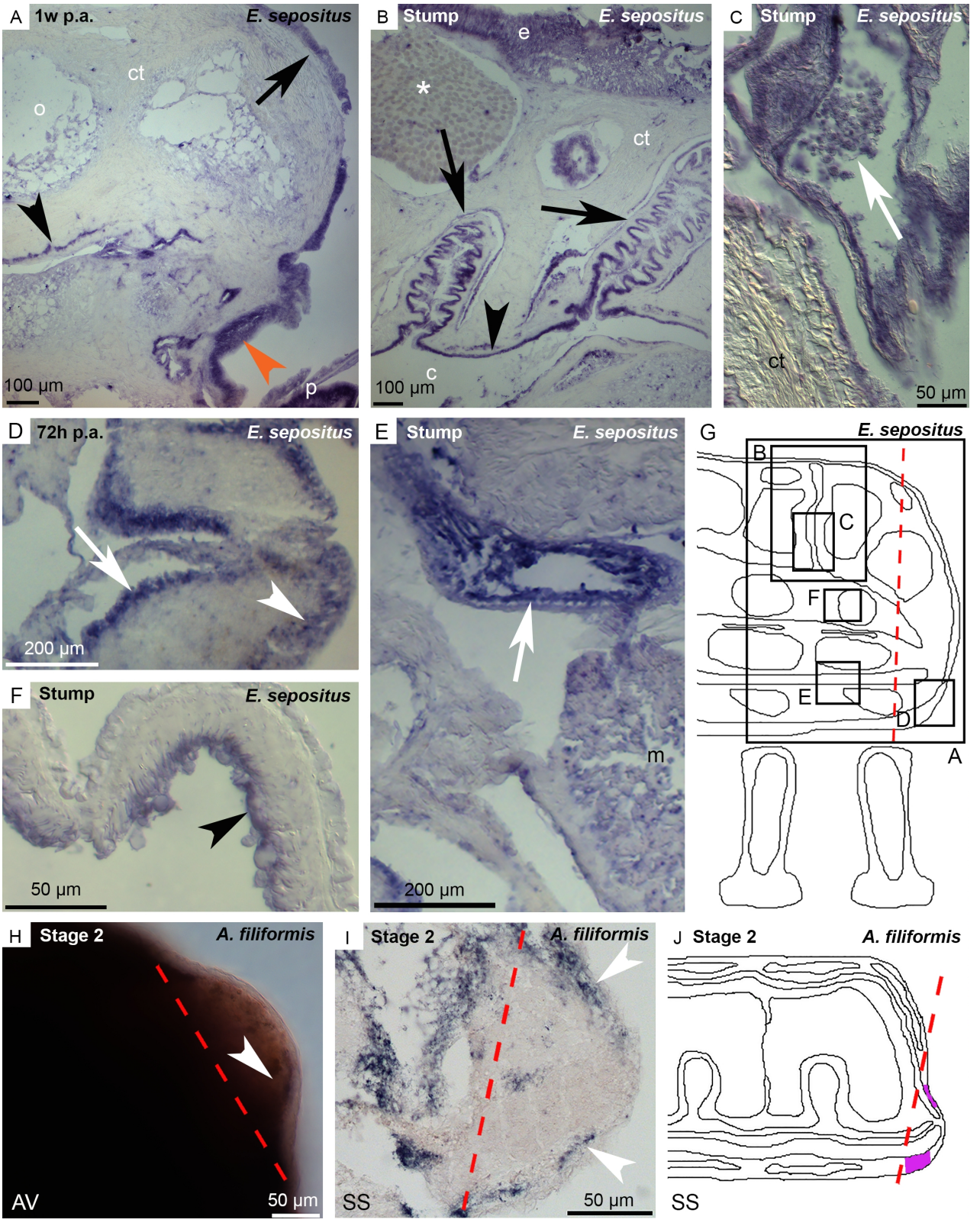
A 1w p.a.
E. sepositus
ct
o
p
100 µm
B Stump
E. sepositus
e
*
ct
c
100 µm
C Stump
E. sepositus
ct
50 µm
D 72h p.a.
E. sepositus
200 µm
E Stump
E. sepositus
m
200 µm
F Stump
E. sepositus
50 µm
G
E. sepositus
B
C
F
E
D
A
H Stage 2
A. filiformis
AV
50 µm
I Stage 2
A. filiformis
SS
50 µm
J Stage 2
A. filiformis
SS

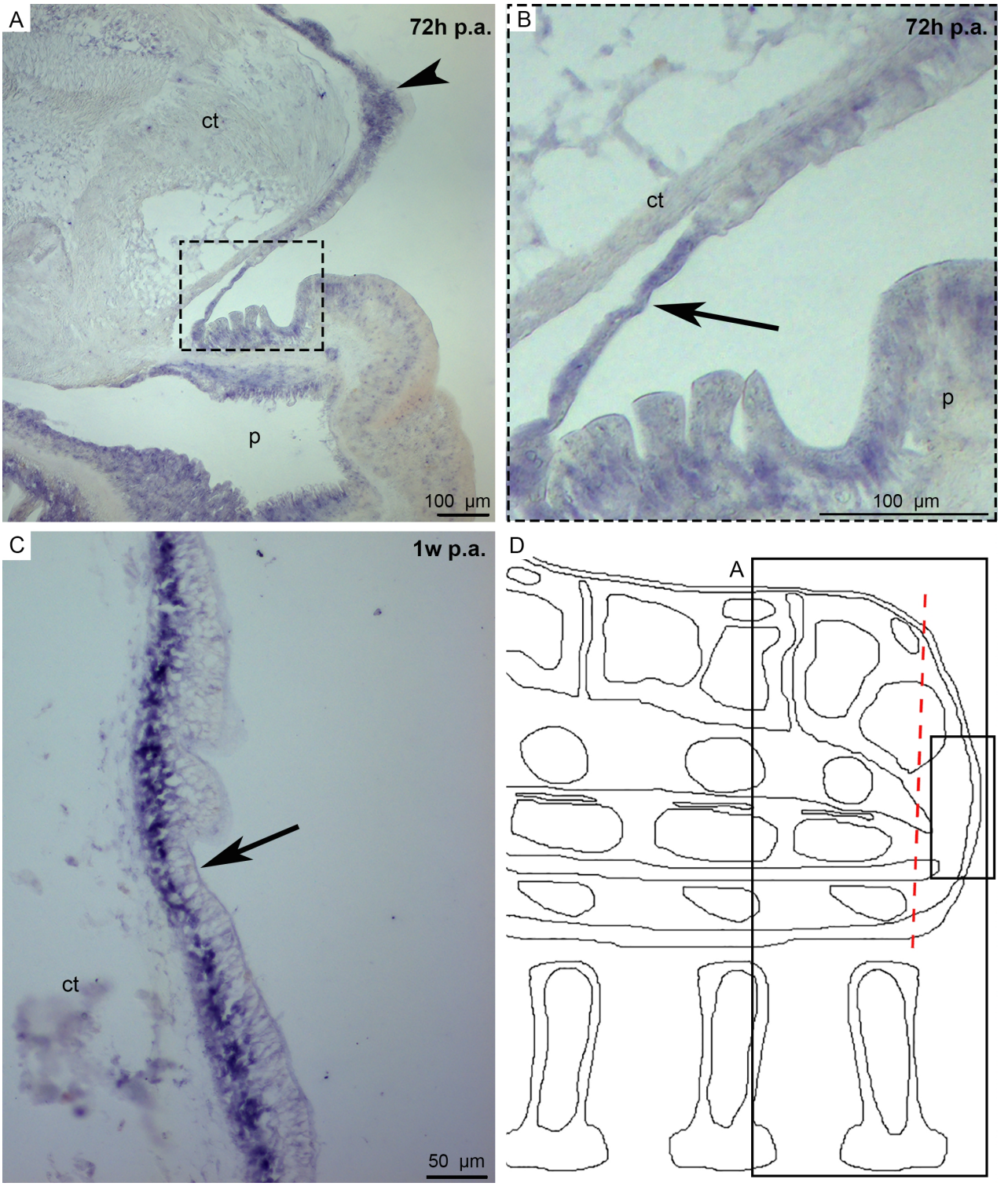
A
72h p.a.
ct
p
100 µm
B
72h p.a.
ct
p
100 µm
C
1w p.a.
ct
50 µm
D
A

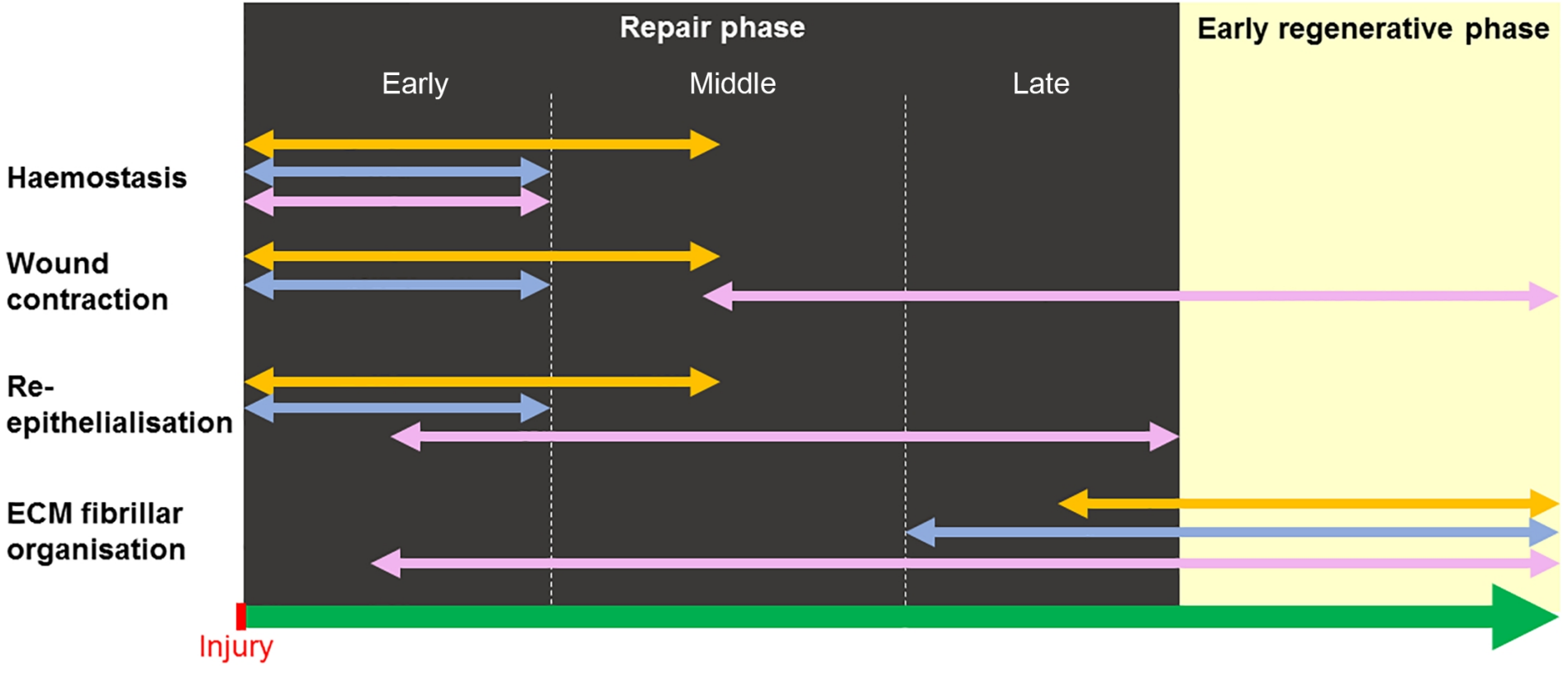


Colour legend: STARFISHES, BRITTLE STARS, MAMMALS

***Supplementary Materials***

## ***1. Extended Materials and Methods***

### *1.1. Microscopy analyses*

#### *1.1.1. Scanning electron microscopy (SEM) of E. sepositus regenerating samples*

After sagittal sectioning, the remaining paraffin embedded half-samples of regenerating arms were used for scanning electron microscopy as described in Ben Khadra and co-workers (2015a, b). Briefly, they were washed several times with xylene followed by absolute ethanol and then transferred to a series of solutions of Hexamethyldisilazane (HMDS) in absolute ethanol in different proportions (1:3, 1:1, 3:1, and 100% HMDS). Finally, they were mounted on stubs, covered by a thin layer of pure gold (Sputter Coater Nanotech) and observed under a scanning electron microscope (LEO-1430).

### *1.2. Gene expression analyses*

#### *1.2.1. 3'RACE and degenerate PCR protocols for E. sepositus cDNA amplification*

For *Ese-actin* standard gradient PCR was performed and the transcript was successfully cloned. However, since the PCR product was short (less than 300 bp), 3'RACE was performed using a mixed cDNA samples from regenerate stages with the FirstChoice® RLM-RACE Kit (Ambion) according to manufacturer's instructions optimising annealing temperature (55°C) and number of cycles (40) in order to obtain a longer product (predicted length ~ 1 kb) and thus a longer RNA antisense probe. Primers used for 3'RACE are listed in Table S3. Also these PCRs were successful, therefore both PCR products were cloned and used to transcribe RNA antisense probes.

For *Ese-ets1/2* degenerate primers (100 µM; see Table S2) were used on a mixed cDNA samples from different regenerative stages as follows: 95°C for 5' followed by 35 cycles of 95°C for 30'', temperature gradient for 30'' and 72°C for 30'' and a final 7' elongation at 72°C. The temperatures of the gradient from the highest to the lowest were: 60°C, 54.5°C, 48°C and 45°C. The amplification was successful for all of them and all PCR products were pooled, cloned and used to obtain the RNA antisense probe as already described.

For *Ese-p4h*, manually designed degenerate primers (100 µM; see Table S2) were used with Q5 High-Fidelity DNA Polymerase (New England BioLabs) and Invitrogen reagents and the following protocol: 98°C for 30'', 35 cycles of 98°C for 10'', temperature gradient for 30'' and 72°C for 30'' and a final 2' elongation at 72°C. After purification with NucleoSpin® gel

and PCR clean-up kit (Macherey-Nagel), cloning and RNA antisense probe transcription were performed as already described.

Collagen-specific degenerate primers (20 µM; see Table S2) from Zhang and Cohn (2006) were used on a mixed cDNA samples from different regenerative stages. To optimise the amplification, the following protocol was tested and subsequently modified: 94°C for 1' followed by 35 cycles of 94°C for 45'', temperature gradient for 45'' and 68°C for 2' and a final 10' elongation at 68°C. The temperatures of the gradient from the highest to the lowest were: 60°C, 54.5°C, 50.8°C and 45°C. 50.8°C was selected as best amplification temperature and cycles were increased to 40. The PCR product was then purified with NucleoSpin® gel and PCR clean-up kit (Macherey-Nagel) and cloned as already described.

**Table S1.** *Best BLAST hits of the identified genes in EchinoBase (SPU Best BLAST) and in NCBI (NCBI Best BLAST) with corresponding scores and E-values.*

| Gene Name | SPU Best BLAST | Score | E-value | NCBI Best BLAST | Score | E-value |
|---|---|---|---|---|---|---|
| ***Ese-actin*** | SPU_009481 | 180 | 2e-46 | actin 1 [*Echinaster sepositus*] KC858258.1 | 187 | 3e-60 |
| ***Ese-ets1/2*** | SPU_002874 | 191 | 9e-50 | ets1/2 transcription factor [*Patiria pectinifera*] BAJ33504.1 | 202 | 3e-61 |
| ***Ese-fib-like*** | SPU_023548 | 153 | 1e-37 | fibrinogen-like protein A [*Amphimedon queenslandica*] XP_003387435.1 | 162 | 2e-44 |
| ***Ese-p4h*** | SPU_014011 | 119 | 3e-28 | prolyl 4-hydroxylase subunit alpha-1 [*Clupea harengus*] XP_012689665.1 | 140 | 5e-37 |
| ***Afi-actin*** | SPU_009481 | 562 | e-160 | actin related protein 1 [*Strongylocentrotus purpuratus*] NP_999634.1 | 581 | 0.0 |
| ***Afi-ficolin*** | SPU_017963 | 215 | 2e-56 | fibrinogen-like protein A-like [*Saccoglossus kowalevskii*] XP_006824721.1 | 214 | 7e-67 |
| ***Afi-p4h*** | SPU_027669 | 86 | 3e-17 | prolyl 4-hydroxylase subunit alpha-1 [*Clupea harengus*] XP_012689665.1 | 120 | 9e-28 |

**Table S2.** *List of E. sepositus (Ese) and A. filiformis (Afi) primers with corresponding primer length.* Abbreviations and symbols*:* bp - base pair; F - forward primer; R - reverse primer; * - degenerate primers; ** - collagen-specific degenerate primers from Zhang and Cohn (2006).

| Primer Name | Primer Sequence (5'-3') | Primer Length (bp) |
|---|---|---|
| ***Ese-actin F*** | GTGCCCAGAAGCCTTGTTC | 19 |
| ***Ese-actin R*** | AGGATAGAGCCACCGATCC | 19 |
| ***Ese-ets1/2 F **** | CA(A/G)GA(A/G)CGNCUNGGNAU(A/C/U)CCNAA(A/G) | 24 |
| ***Ese-ets1/2 R **** | (A/G)TC(A/G)CANAC(A/G)AANCG(A/G)TANAC(A/G)TA | 24 |
| ***Ese-fib-like F ***** | GGCCCTCCCGGCCTGCARGGNATGCC | 26 |
| ***Ese-fib-like R ***** | GGGGCCGATGTCCACGCCRAAYTCYTG | 27 |
| ***Ese-p4h F **** | GGNCAYTAYGARCCNCAYTTYGAY | 24 |
| ***Ese-p4h R **** | DATCCADATRTTNGCNACCCAYTT | 24 |
| ***Afi-actin F*** | ACGACGAAGTATCCGCTTTG | 20 |
| ***Afi-actin R*** | TCGCATTTCATGATGCTGTT | 20 |
| ***Afi-ficolin F*** | CGATGGACATGATGGAAATG | 20 |
| ***Afi-ficolin R*** | GAGGGCCGCCAAGATATAAT | 20 |
| ***Afi-p4h F*** | TCTCCAATCATGGGCCTACT | 20 |
| ***Afi-p4h R*** | ACAGGTTTGCAGCCCATTT | 19 |

**Table S3.** *List of 3' outer and inner primers used for E. sepositus 3'RACE PRCs (FirstChoice® RLM-RACE Kit; Ambion) for Ese-actin.* All primers were used at a concentration of 10 µM. Abbreviations and symbols: bp - base pair; F - forward primer; R - reverse primer; * - specific F primer already present in Table S2.

| Primer Name | Primer Sequence (5'-3') | 3' RLM-RACE PCR | Primer Length (bp) |
|---|---|---|---|
| ***Ese-actin SO**** | GTGCCCAGAAGCCTTGTTC | Specific outer | 19 |
| ***Ese-actin SI*** | CATCATGAAGTGTGACGTGGA | Specific inner | 21 |
| ***3' RACE inner*** | CGCGGATCCGAATTAATACGACTCACTATAGG | Kit inner primer | 32 |
| ***3' RACE outer*** | GCGAGCACAGAATTAATACGACT | Kit outer primer | 22 |

*1.2.2. Whole mount in situ hybridisation (WMISH)*

For each stage at least three *A. filiformis* regenerating arms from different experimental animals were used to test each RNA antisense probe. Samples were re-hydrated in a decreasing scale of ethanol in DEPC-treated water and then washed three times in 1X MABT (0.1 M maleic acid pH 7.5, 0.15 M NaCl, 0.1% Tween-20). A wash with 1:1 (v/v) 1X MABT and hybridisation buffer (HB; 50% de-ionized formamide, 0.02 M Tris pH 7.5, 10% PEG, 0.6 M NaCl, 0.5 mg/ml yeast RNA, 0.1% Tween-20, 5 mM EDTA, 1X Denhardt's) was performed and then samples were incubated in HB for one hour at 50°-55°C. The HB was replaced with 0.02 ng/µl probes in HB and left to hybridise for five days at 50°C-55°C. After this period 250 µl of 1X MABT and 250 µl of HB were added and one wash with 1:1 (v/v) 1X

MABT and HB was performed, followed by a wash of 10 minutes with 75% 1X MABT/25% HB. Two washes with 1X MABT were then followed by two washes with 0.1X MABT supplemented with 0.1% Tween-20. All these washes were performed at 50°C-55°C. Samples were incubated with blocking buffer (BB; 5% goat serum in 1X MABT) for 30 minutes and then for one hour at RT (or ON at 4°C) in 1:1000 alkaline phosphates conjugated antibody anti-DIG (Roche) in BB. Five washes were then performed with 1X MABT, followed by two washes with the freshly prepared alkaline phosphatase buffer (AP; 0.1 M Tris pH 9.5, 0.1 M NaCl, 0.05 M MgCl2, 0.1% Tween-20, 1 mM Levamisole). Then, the staining reaction was developed using 10 µl NBT/BCIP mix (Roche) with 10% dimethylformamide in AP. The detection of the staining was monitored under the stereomicroscope. The reaction was stopped with one wash in 1X MABT with 0.5 M EDTA followed by three washes (5 minutes each) in 1X MABT. Then a quick wash with 1:1 (v/v) 1X MABT and 50% glycerol was performed and samples were stored in 50% glycerol till observation.

*1.2.3. In situ hybridisation (ISH) on paraffin sections*

Two different ISH protocols were optimised and performed on starfish paraffin sections. Moreover, since it was the first time that ISH was performed on *E. sepositus* sections negative controls were performed as well (see Extended Results).

The first protocol was modified from the WMISH protocol used for *A. filiformis* samples (see above). Sections were warmed up 30 minutes at 55°C and cooled down at RT for 15 minutes. Slides were de-waxed with Histoclear and rehydrated in a decreasing scale of ethanol in DEPC-treated water, washed twice in 1X MABT and post-fixed in 4% PFA in 1X MABT for 20 minutes at RT. After one wash in 1X MABT supplemented with 0.1% Tween-20, slides were washed in 1:1 solution of 1X MABT and HB for 5 minutes at RT. Then, slides were pre-hybridised in HB for one hour at 45°-55°C. Probes in HB were subsequently added at a final concentration ranging from 0.02 to 1 ng/µl and left for one or five days at 45°-55°C in humid chamber. The following steps (*i.e.* washes post-hybridisation, blocking, antibody exposure and staining) were performed as described for brittle star samples (see above). When staining was complete the reaction was stopped with one wash in 1X MABT with 0.5 M EDTA followed by three washes in 1X MABT. Finally, slides were mounted with 50% glycerol and stored at RT till observation.

The second protocol was described by Etchevers and co-workers (2001) and modified by Gillis and co-workers (2012). Briefly, slides were de-waxed with Histoclear (two times for 5

minutes) and rehydrated in a decreasing series of ethanol in DEPC-treated 1X PBS. They were subsequently rinsed in DEPC-treated water, DEPC-treated 1X PBS with 0.1% Tween-20 and 2X SSC solution. Probes were added to the hybridisation mix at a concentration of 1 ng/µl (1X salt solution, 50% formamide, 10% dextran sulfate, 1 mg/ml yeast tRNA, 1X Denhardt's solution in DEPC-treated water; salt solution: 0.2 M NaCl, 0.89 mM Tris HCl, 0.11 mM Tris base, 5 mM $NaH_2PO_4xH_2O$, 5 mM $Na_2HPO_4$, 5 mM EDTA) and slides were incubated under glass coverslips at 65°-70°C ON in a humid chamber. Two washes of 30 minutes each in pre-warmed 50% formamide, 1X SSC and 0.1% Tween-20 were performed at 65°-70°C in order to remove the coverslips and slides were then washed three times for 10 minutes in 1X MABT at RT. Slides were subsequently blocked for two hours at RT in 1% Roche blocking reagent in 1X MABT with 20% sheep serum (Sigma-Aldrich). Later on, 1:1000 anti-DIG-AP in the same solution was added and left ON at RT in humid chamber covered with wax coverslips. Slides were washed four-five times in 1X MABT and then equilibrated in NTMT (0.1 M NaCl, 0.1 M Tris pH 9.5, 5 mM $MgCl_2$ and 0.1% Tween-20 in milliQ water). Staining was performed by adding BM Purple AP substrate (Roche) at RT in the dark and stopped with 1X PBS. Slides were post-fixed for 5 minutes in 4% PFA in 1X PBS, washed with 1X PBS and mounted with DAPI Fluoromount-G® (SouthernBiotech).

## *2. Extended results*

### *2.1. Gross morphology of starfish and brittle star non-regenerating arms*

Starfish arms (Fig. S1A) are mainly occupied by a spacious perivisceral coelom containing the pyloric caeca and the ampullae, the inner outgrowths of the podia. Two rows of podia, located on the oral surface, run along the whole arm together with the radial water canal and the radial nerve cord. The body wall is mainly occupied by calcitic ossicles and spines embedded in an abundant dermal layer and joined by muscle bundles.

Brittle star arms (Fig. S1B) are subdivided in repetitive segments, each one mainly occupied by a set of skeletal elements, namely the central vertebra, the inner aboral, oral and lateral shields and the external spines, all embedded in a thin dermal layer. Muscle bundles and ligaments link the adjacent segments. The aboral coelomic cavity (much reduced if compared to that of starfishes), the radial water canal and the radial nerve cord uninterruptedly run along the whole arm length. Differently from starfishes, the digestive tract is not hosted in the arm.

For further details of *E. sepositus* arm anatomy see Ben Khadra and co-workers (2015a) and for *A. filiformis* see Biressi and co-workers (2010) and Czarkwiani and co-workers (2016).

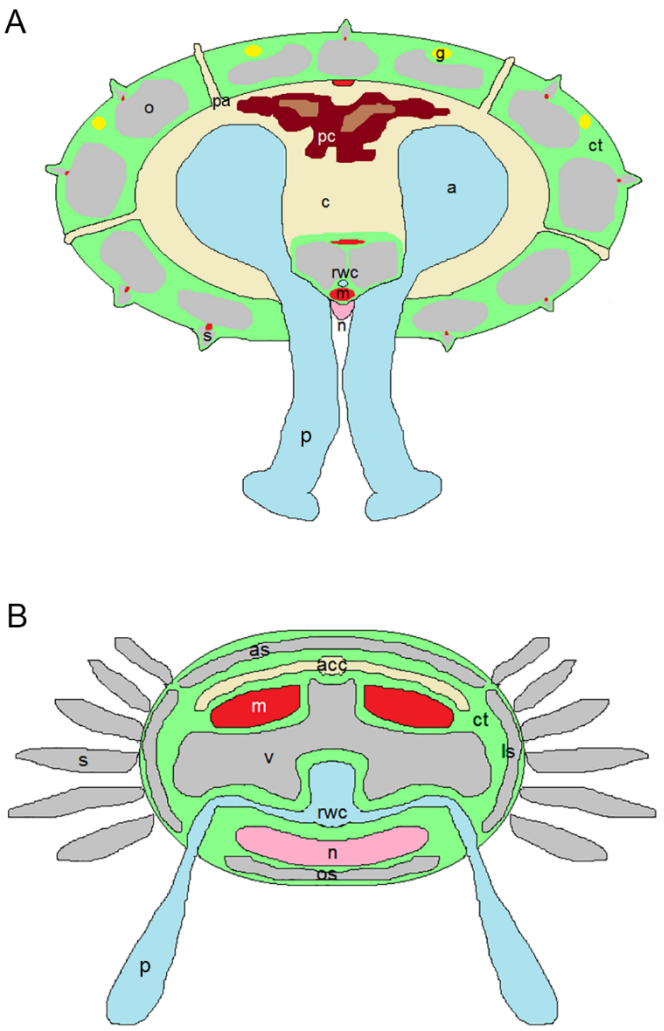


ABBREVIATIONS' LEGEND:

a: ampulla
acc: aboral coelomic cavity
as: aboral shield
c: coelom
ct: connective tissue
g: mucous gland
ls: lateral shield
m: muscle
n: radial nerve cord
o: ossicle
os: oral shield
p: podium
pa: papula
pc: pyloric caeca
rwc: radial water canal
s: spine
v: vertebra

**Fig. S1.** Gross morphology of the arms of the two echinoderm models. A) Schematic cross section of an arm of *Echinaster sepositus*. B) Schematic cross section of an arm of *Amphiura filiformis*. Abbreviations' legend is embedded in the figure.

*2.2. Main events of E. sepositus repair phase*

The main events of the repair phase are here re-called in Fig. S2. For a detailed description see Ben Khadra and co-workers (2015a, b).

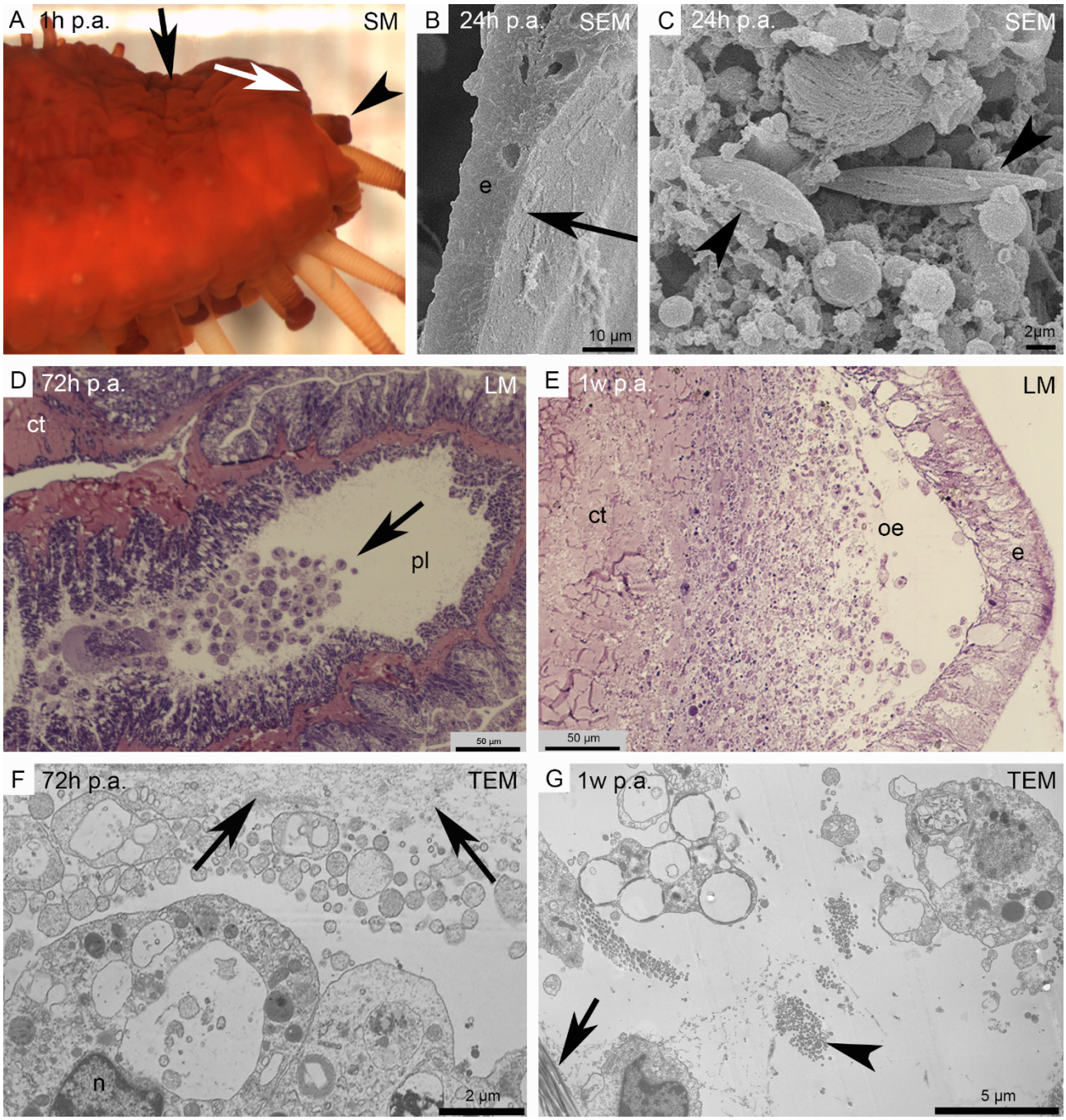


**Fig. S2.** *Main events of E. sepositus repair phase*. A) Stereomicroscope (SM) lateral view of the arm stump. The haemostatic ring (circular constriction) is visible (black arrow) immediately behind the amputation plane. The first pair of podia (arrowhead) is contracted at the level of the injury in order to help wound closure by reducing its surface. The aboral body wall moves toward the oral side (white arrow). B) Scanning electron microscopy (SEM) sagittal view of the new epidermis. C) SEM sagittal view of the clot underneath the new epidermis composed of different cytotypes: roundish cells (possibly phagocytes) and spindle-like cells (dedifferentiating myocytes; arrowheads). D) Semi-thin sagittal section of

a papula far from the amputation plane showing circulating cells (presumptive coelomocytes) that are possibly recruited for regeneration. E) Semi-thin parasagittal section of the regenerating arm where the oedematous area is visible underneath the new epidermis. Cells and newly-deposited ECM are detectable. F) TEM micrograph of the oedematous area where cells are immersed in a nonfibrillar collagenous material (arrows). G) TEM micrograph of the oedematous area where more numerous new collagen fibrils in cross section (arrowhead) and longitudinal section (arrow) are visible spread among oedematous cells. Abbreviations: ct - connective tissue; e - epidermis; LM - light microscopy; n - nucleus; oe - oedematous area; pl - papula lumen; SEM - scanning electron microscopy; TEM - transmission electron microscopy.

### *2.3. Extended ISH results*

For both echinoderm species the gene expression patterns in the stump was evaluated as well since its tissues are in close continuity with the regenerating tissues and might therefore be important during the regenerative process. Moreover, although not strictly relevant for the repair phase, in some cases the signal in the advanced regenerative stages of *A. filiformis* was considered to confirm/validate the results obtained in the early stages and have a more complete overview of the expression pattern of the identified genes throughout regeneration. Thus, expressions of *Afi-ficolin*, *Ese-p4h* and *Afi-p4h* are described below.

The analysis of *Afi-ficolin* expression pattern reveals a strong signal in the stump radial water canal epithelium (Fig. S3). This gene is detectable in the early regenerative phase after injury in the stump and in the regenerating tissues (Fig. 4) suggesting that it is likely to be involved in the repair/early regenerative phases, in line with its immunity-related function.

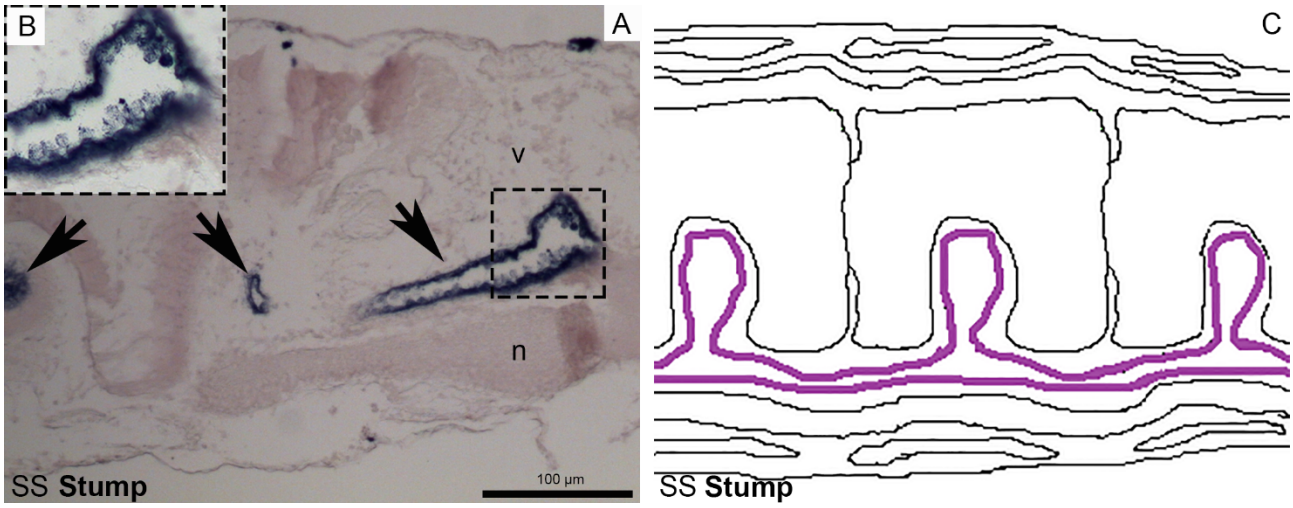


**Fig. S3.** *Afi-ficolin expression pattern in the A. filiformis stump tissues.* A-B) Paraffin sagittal sections. C) Sagittal section scheme. *Afi-ficolin* is expressed in the radial water canal epithelium (arrows). Abbreviations: n - radial nerve cord; SS - sagittal section; v - vertebra.

In the stump tissues, *Ese-p4h* is present in the coelomic epithelium lining the perivisceral coelom, the papulae and the radial water canal, in the pyloric caeca and in the ectoneural and hyponeural systems of the radial nerve cord (Fig. S4A-C).

Considering *Afi-p4h*, in the stump tissues it is localised in the inner coelomic lining of the podia (Fig. S4D). At stage 2 the blueish staining visible in the new epidermis is background (Fig. S4E). In the >50% stages at the proximal side a true signal is localised in the aboral coelomic cavity epithelium, whereas blueish staining detectable in the podia and spine epidermis is background staining (Fig. S4F-I).

Overall, considering both experimental models the *p4h* gene is consistently expressed, even if at different stages, only in the coelomic lining suggesting a possible involvement of these tissue in collagen biosynthesis.

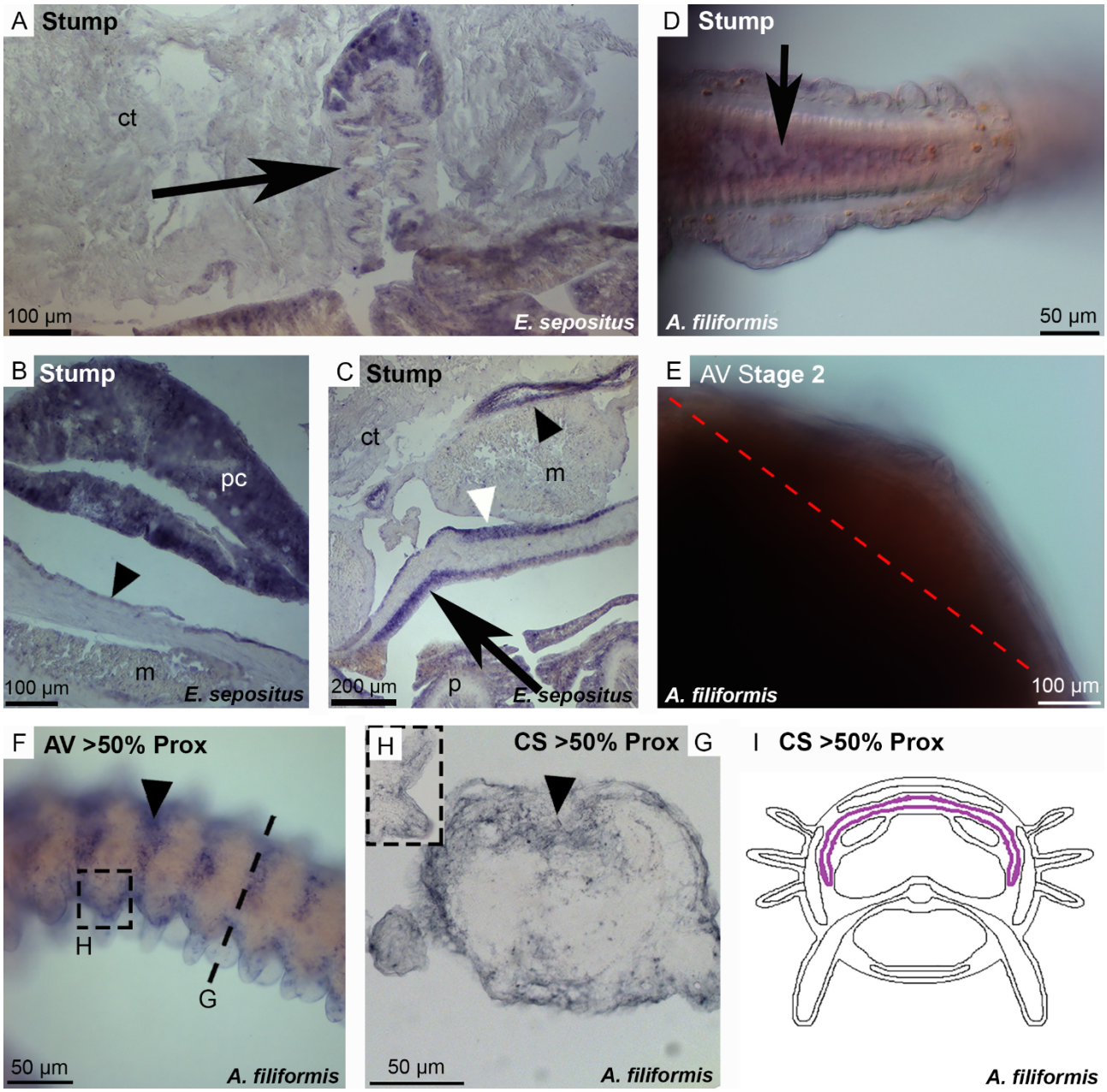


**Fig. S4.** *Expression pattern of Ese-p4h in the E. sepositus stump tissues and of Afi-p4h in the A. filiformis stump tissues and advanced regenerative stages.* A-C: *E. sepositus*; D-I: *A. filiformis*. A) *Ese-p4h* is expressed in the coelomic lining of the papulae (arrow). B) A signal is visible in the coelomic lining of the perivisceral cavity (arrowhead) and in the pyloric caeca. C) *Ese-p4h* is expressed in the coelomic lining of the radial water canal (black arrowhead), and in the ectoneural (arrow) and hyponeural (white arrowhead) systems of the radial nerve cord. D) *Afi-p4h* is expressed in the inner lining of the stump podium (arrow). E) At stage 2 the blueish staining visible in the epidermis is just background due to long staining step. F) *Afi-p4h* is expressed in the aboral coelomic cavity epithelium (arrowhead). The blueish staining in the epidermis covering spines and podia is background. G) Cross section of F showing the staining in the aboral coelomic cavity epithelium (arrowhead). The blueish staining in the epidermis is background. H) The blueish staining in the spine epidermis is background. I) Cross section scheme showing *Afi-p4h* expression pattern (violet). Abbreviations: AV - aboral view; CS - cross section; ct - connective tissue; m - muscle; p -

podium; pc - pyloric caeca; Prox - proximal. Red dotted line - amputation plane. Black dotted lines - level corresponding to the cross sections shown in Fig. G.

*2.4. Expression of actin and ets1/2 genes in E. sepositus and A. filiformis*

*Actin* and *ets12* were selected as positive controls in both species in order to validate the ISH protocols and be confident of the technique, especially for *E. sepositus*. The detailed expression patterns of *Ese-actin*, *Afi-actin* and *Ese-ets1/2* in both stump and regenerating tissues are described below. For *Afi-ets1/2* see Czarkwiani and co-workers (2013).

*Ese-actin* is a transcript whose sequence is available in NCBI (GenBank: KC858258.1, around 300 bp long; see Table S1). This is referred to as *actin 1* and the actin domain was confirmed by cDART tool (NCBI). The sequence of the *actin* obtained through 3'RACE PCR has been checked as well, confirming the previous result. In the regenerating area *Ese-actin* is present in the new epidermis (Fig. S5G), the regenerating radial nerve cord and radial water canal (Fig. S5H). In the stump tissues the signal is detectable in the coelomic lining of the perivisceral cavity (Fig. S5A), the papulae (Fig. S5B), the ampullae (Fig. S5C) and the podia (Fig. S5D) and in the pyloric caeca (Fig. S5A). Moreover, it is present also in the epidermis of the podia (Fig. S5D) and of the body wall (Fig. S5E) and in the non-regenerating radial nerve cord, in particular in the ectoneural and hyponeural systems (Fig. S5F).

For *Afi-actin* (*Afi*CDS.id2787.tr9243) the best BLAST hit in the sea urchin database (EchinoBase) is *Sp-Cska1* (SPU_009481) also called *Cyl*, whereas from the NCBI non-redundant database is an actin related protein 1 [*Strongylocentrotus purpuratus*] (NP_999634.1; see Table S1). Therefore, this transcript was considered as *actin*. Both WMISH and post *in situ* sections show that *Afi-actin* is expressed in the regenerative bud epidermis at stage 2 (Fig. S6A, F, I). The same expression pattern is detectable at stage 4 (Fig. S6B, G, J). At >50% stages, *Afi-actin* is expressed in the proximal side of the long regenerate in the epidermis covering spines and podia (Fig. S6C, D, H, K) and not the other structures (*i.e.* oral, aboral and lateral sides). In the distal tip this transcript is expressed in the epidermis as well (Fig. S6E, I, L).

In general, in both experimental models a consistent signal of actin is detectable only in the epidermis in both stump and regenerating tissues.

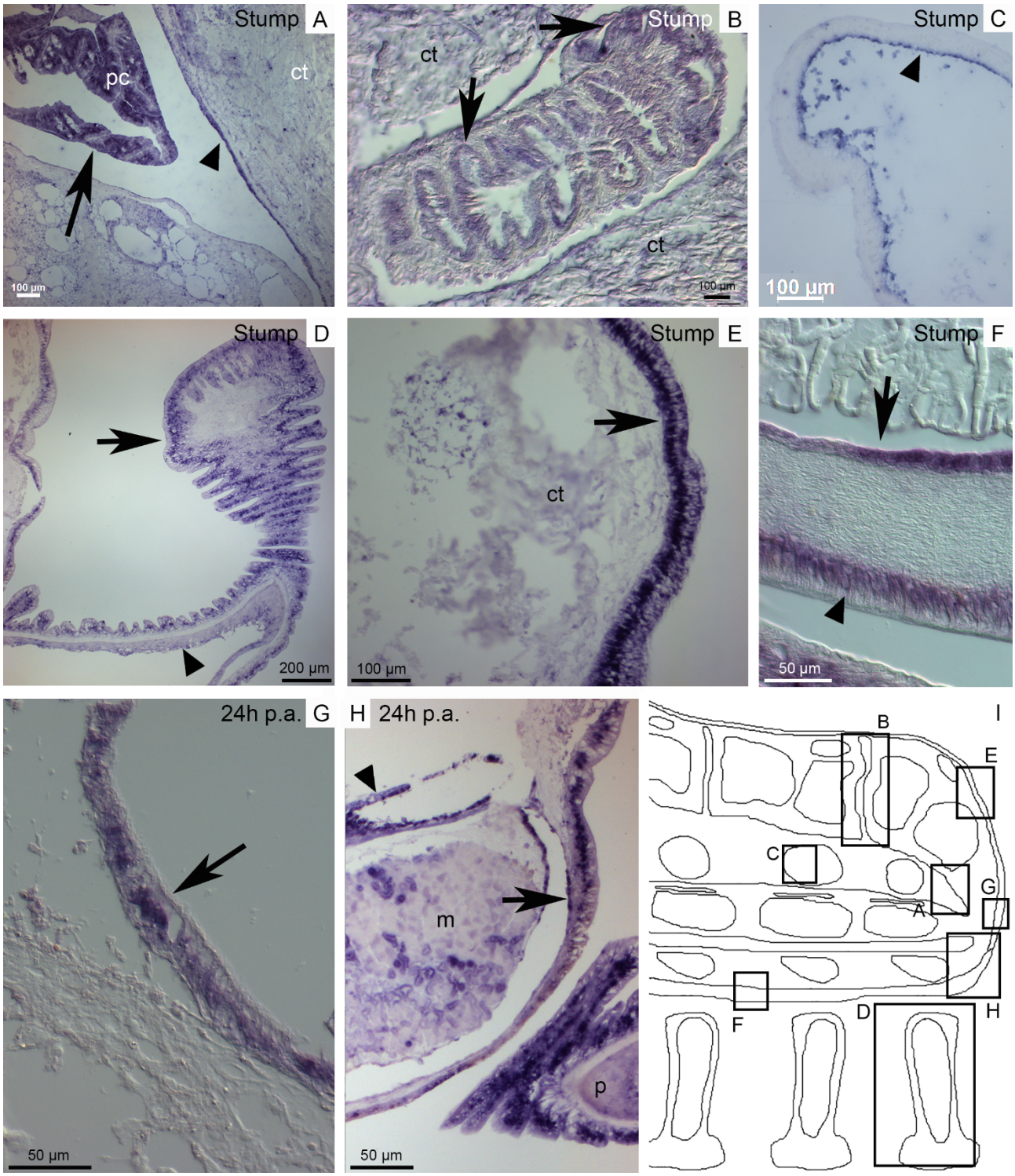


**Fig. S5.** *Expression pattern of Ese-actin on E. sepositus stump tissues and regenerating arms.* A) *Ese-actin* is expressed in the coelomic cavity epithelium (arrowhead) and in the pyloric caeca (arrow) of the stump. B) The inner lining of the stump papulae (*i.e.* coelomic epithelium) shows expression of this transcript (arrows). C) *Ese-actin* is expressed in the inner lining of the stump ampulla (*i.e.* coelomic epithelium; arrowhead). D) *Ese-actin* is expressed in the epidermis of the stump podia (arrow) and in the inner coelomic lining (arrowhead). E) *Ese-actin* is expressed in the epidermis of the stump (arrow). F) *Ese-actin* shows an expression in the stump radial nerve cord, in particular in the ectoneural (arrowhead) and in the hyponeural systems (arrow). G) *Ese-actin* is expressed in the new epidermis (arrow). H) The regenerating radial nerve cord (arrow) and radial water canal

epithelium (arrowhead) show a signal. I) Sagittal section scheme of the starfish regenerating arm where the black boxes indicate corresponding images of this figure to facilitate the understanding of the expression pattern location. Abbreviations: ct - connective tissue; m - lower transverse ambulacral muscle; p - podium; pc - pyloric caeca.

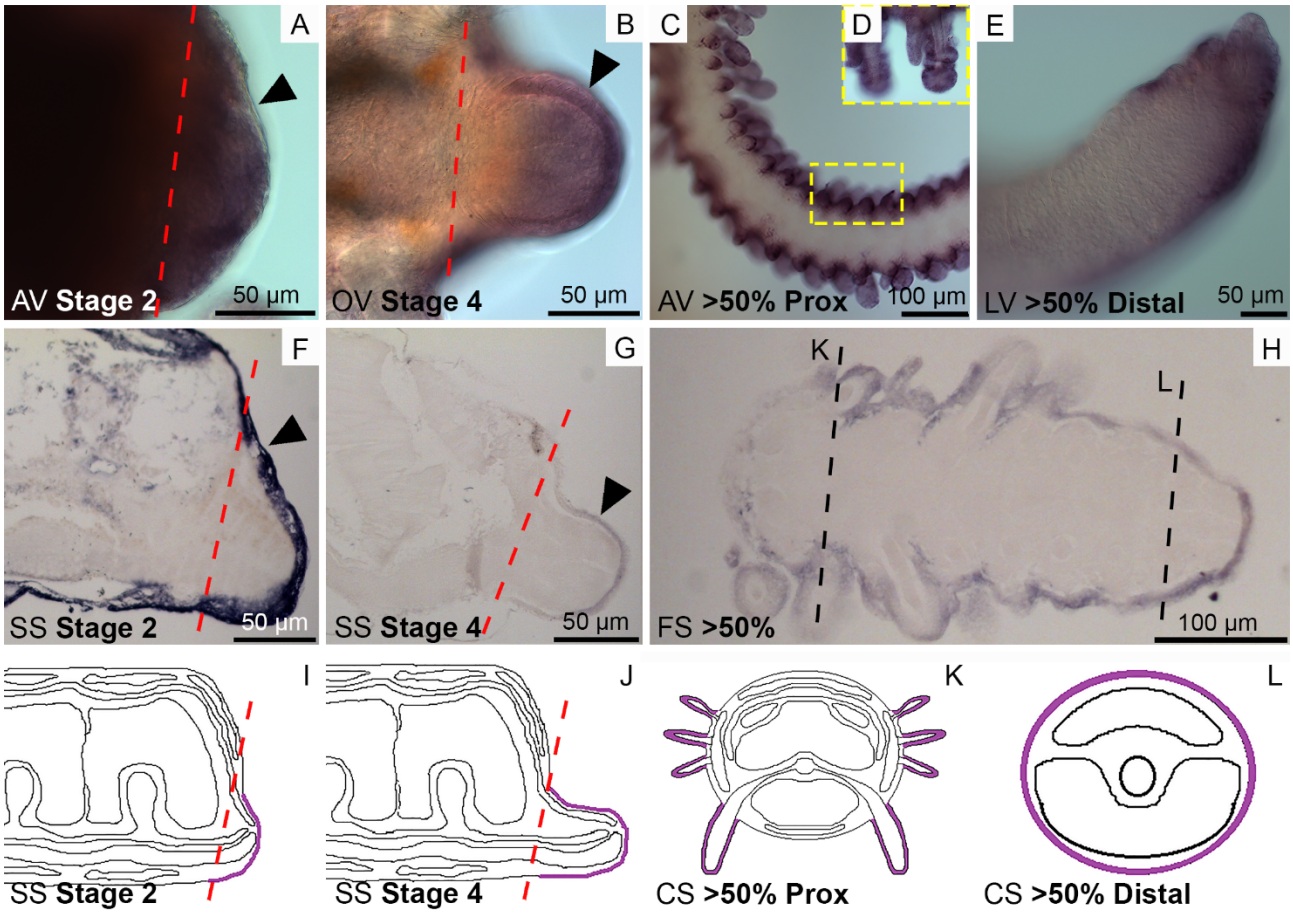


**Fig. S6.** *Afi-actin expression pattern at different A. filiformis regenerative stages*. 1st line: WMISH; 2nd line: post *in situ* sectioning; 3rd line: schemes. Stage 2: A, F, I. *Afi-actin* is expressed in the epidermis (arrowheads) of the regenerative buds. Stage 4: B, G, J. *Afi-actin* is expressed in the epidermis (arrowheads) of the regenerates. Stage >50%: C, D, E, H, K, L. *Afi-actin* is expressed in the proximal side at the level of the spine and podia epidermis, whereas in the distal side is expressed in the whole epidermal layer. Abbreviations: AV - aboral view; CS - cross section; FS - frontal section; LV - lateral view; OV - oral view; Prox - proximal; SS - sagittal section. In the schemes the gene expression pattern is shown in violet. Red dotted lines - amputation plane. Black dotted lines - level corresponding to the cross section schemes shown in Fig. K and L.

After cloning through degenerate PCR, *Ese-ets1/2* sequence was checked with NCBI BLAST-X (*vs* non-redundant database) and it showed 100% identity with *ets1/2* transcription factor of the starfish *Patiria pectinifera* (see Table S1). Moreover, using cDART tool (NCBI) the *ets* domain was detected. Therefore, this transcript was confirmed being the transcription factor *ets1/2*. *Ese-ets1/2* is expressed in the stump in the epidermis of body wall and podia (Fig. S7A). The coelomic epithelium presents a signal in the inner lining of the podia (Fig.

S7A), the radial water canal (Fig. S7F), the papulae (Fig. S7B), the ampullae (Fig. S7G) and the perivisceral coelom in both the stump area (Fig. S7D) and the regenerating area (Fig. S7E). This transcript is localised also in the pyloric caeca (Fig. S7D) and in the stump radial nerve cord, particularly in the ectoneural and hyponeural systems (Fig. S7F). The new epidermis shows a signal as well (Fig. S7C). No expression is visible in the main muscle bundles (Fig. S7F) and ossicles (Fig. S7A, C). Contrary to what described in *A. filiformis* (Czarkwiani *et al.*, 2013), in *E. sepositus* no signal is detectable in the dermal layers where ossicles are present. Overall, the *ets1/2* probe in starfishes shows discrete localisation in the regenerating epidermis, in the stump coelomic lining of different coelomic structures and in the stump radial nerve cord.

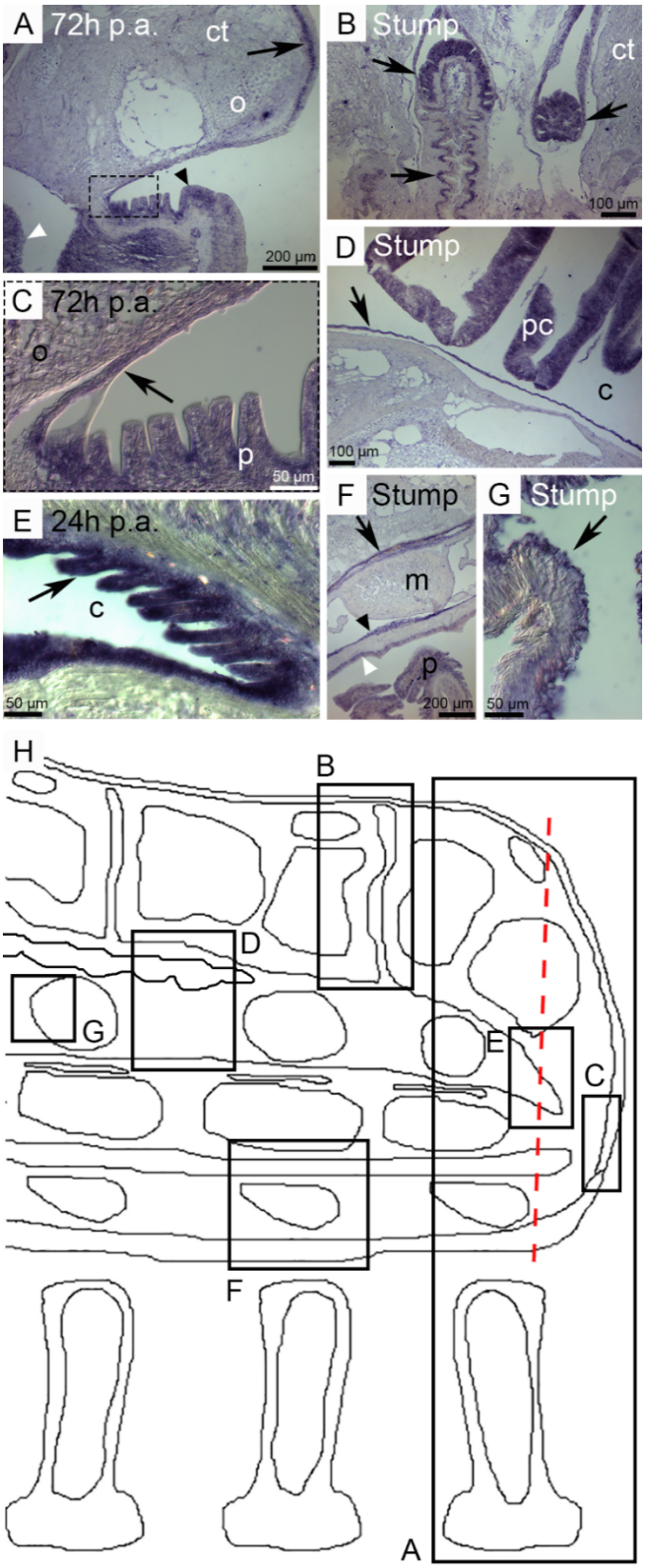


**Fig. S7.** *Expression pattern of Ese-ets1/2 on E. sepositus stump tissues and regenerating arms.* A) *Ese-ets1/2* is expressed in the stump at the level of the epidermis (arrow) and of the podium, in particular in the epidermis (black arrowhead) and in the inner coelomic lining (white arrowhead). B) The inner lining of the stump papulae (arrows) shows a signal. C) The new epidermis (arrow) shows expression of this transcript. D) *Ese-ets1/2* is expressed in the pyloric caeca and in the coelomic epithelium (arrow). E) This transcript is expressed in the

new coelomic epithelium (arrow). F) In the stump the radial water canal epithelium (arrow) and the radial nerve cord show a clear expression pattern. In particular, in the radial nerve cord both the ectoneural (white arrowhead) and the hyponeural (black arrowhead) systems show a signal. G) The inner lining of the ampullae (arrow) shows expression of this transcript. H) Sagittal section scheme of the starfish regenerating arm where the black boxes indicate corresponding images to facilitate the understanding of the expression pattern location. Abbreviations: c - coelom; ct - connective tissue; m - muscle; o - ossicle; p - podium; pc - pyloric caeca.

*2.5. Negative controls in E. sepositus and A. filiformis*

Since ISH protocol was performed for the first time on *E. sepositus* paraffin sections, negative controls were run to evaluate staining specificity. No signal was detected in different tissues (Fig. S8), therefore signal specificity was confirmed. For negative controls in *A. filiformis* see Czarkwiani and co-workers (2013).

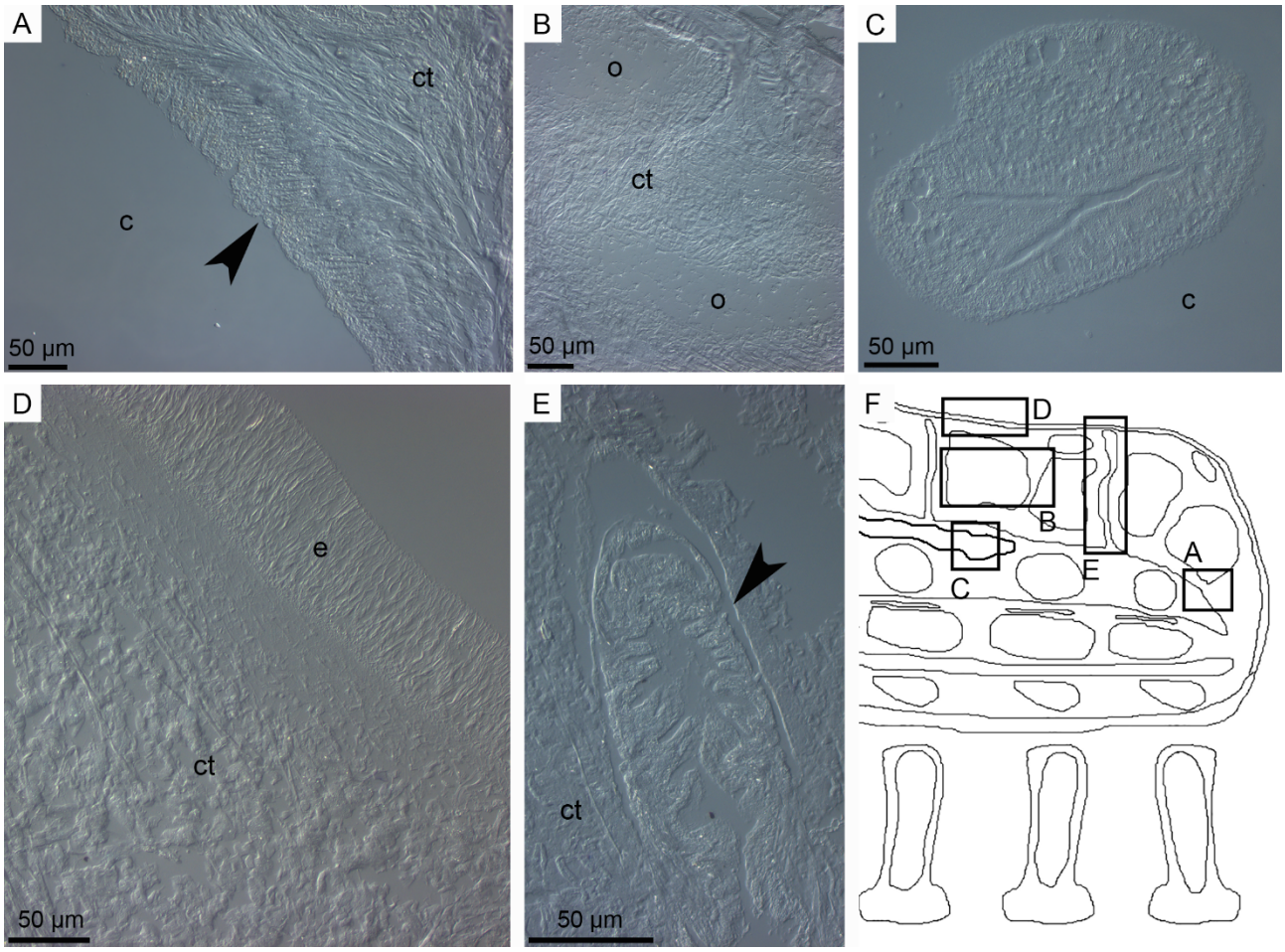


**Fig. S8.** *Negative control of ISH on E. sepositus paraffin sections (stump of a one week p.a. sample).* As expected, in all tissues analysed no signal is detectable. A) Coelomic epithelium (arrowhead). B) Ossicles and connective tissue. C) Pyloric caeca. D) Epidermis and connective tissue. E) Papula. F) Sagittal section scheme of the starfish regenerating arm where the black boxes indicate corresponding images to facilitate the understanding of the location of the shown sections. Abbreviations: c - coelom; ct - connective tissue; e - epidermis; o - ossicle.